A Reproduced Copy

OF

Reproduced for NASA

by the

NASA Scientific and Technical Information Facility

DEPARTMENT OF MECHANICAL ENGINEERING AND MECHANICS
SCHOOL OF ENGINEERING
OLD DOMINION UNIVERSITY
NORFOLK, VIRGINIA

STUDIES ON THE INTERFERENCE OF WINGS AND PROPELLER SLIPSTREAMS

By

Ramadas K. Prabhu

and

Surendra N. Tiwari, Principal Investigator

Final Report
For the period ending December 31, 1984

Prepared for the
National Aeronautics and Space Administration
Langley Research Center
Hampton, Virginia 23665

Under
Research Grant NCC1-65
Dr. Chen-Huei Liu, Technical Monitor
LSAD-Analytical Methods Branch

May 1985

DEPARTMENT OF MECHANICAL ENGINEERING AND MECHANICS
SCHOOL OF ENGINEERING
OLD DOMINION UNIVERSITY
NORFOLK, VIRGINIA

STUDIES ON THE INTERFERENCE OF WINGS AND PROPELLER SLIPSTREAMS

By

Ramadas K. Prabhu

and

Surendra N. Tiwari, Principal Investigator

Final Report
For the period ending December 31, 1984

Prepared for the
National Aeronautics and Space Administration
Langley Research Center
Hampton, Virginia 23665

Under
Research Grant NCC1-65
Dr. Chen-Huei Liu, Technical Monitor
LSAD-Analytical Methods Branch

Submitted by the
Old Dominion University Research Foundation
P. O. Box 6369
Norfolk, Virginia 23508

May 1985

PREFACE

This report covers the work completed on the research project "Wing Propeller Interference Studies." The work was supported by the NASA/Langley Research Center, Analytical Methods Branch of the Low-Speed Aerodynamics Division, through Cooperative Agreement NCC1-65. The project was monitored by Dr. Chen-Huei Liu, LSAD-Aerodynamics Methods Branch, NASA/Langley Research Center.

TABLE OF CONTENTS

LIST OF FIGURES

LIST OF SYMBOLS

AR	Wing aspect ratio
a	Distance of the airfoil below a surface of velocity discontinity
a, a_1, a_2	Parameters appearing in the expression for the nonuniform velocity profile
a_n	Ratio of image vortex strength to actual vortex strength
b	Distance of the airfoil above a surface of velocity discontinuity
b	Wing span
c	Airfoil chord
c(y), c(i)	Chord of wing section
c_o	Wing centerline chord
c_ℓ	Lift coefficient
c_m	Pitching moment coefficient about airfoil leading edge
c_{ℓ_α}	Slope of lift curve
C_L	Total lift coefficient of wing
d, d_1, d_2, d_3	Parameters appearing in the expression for nonuniform velocity profile
$F(r^2)$	A given even function of r
h	Height of a uniform jet
i, j, k, ℓ, n, s	Running indices
I_s J_s K, K_s, $K(n,s)$ L_s	Strength of image vortices

LIST OF SYMBOLS (CONTINUED)

ℓ	Spanwise extent of multiple slipstream
$m(x)$	Slope of mean camber line of an airfoil
p_0, p_1	Static pressure disturbances
R	Radius of slipstream
r	Radial distance from the jet axis
s	Wind semispan
u, u_0, u_1	Velocity disturbances
U, $U(y,z)$	Nonuniform velocity in the axisymmetric jet
U_J, U_0, U_1,...	Velocity in uniform jet
U_∞	Free stream velocity
v	Downwash velocity in two-dimensional flow
v_0, v_1	Velocity disturbances
V	Velocity vector
w, $w(y)$, $w(i)$	Downwash velocity due to wing trailing vortices
x	Distance along X-axis
y, y_1	Distances along Y-axis
α	Angle of attack of airfoil
β	Streamline deflection angle defined on page 11
α_n, β_n	Factors defined on page 16
γ	Srength of a discrete trailing vortex
$\gamma(x)$	Vorticity distribution along the airfoil chord
$\gamma(x,y)$	Vorticity distribution on the jet sheet
ϵ	The ratio c_0/s, assumed to be small
μ,ν	Factors defined on page 13
Γ	Circulation

LIST OF SYMBOLS (CONTINUED)

$\Gamma(y)$	Circulation distribution along the wing lifting line
$\Gamma_J(y)$	Spanwise distribution of additional circulation to account for the inclination of the jet sheet at the lifting line
ϕ	Angular coordinate
Φ, Φ_1	Velocity potential
θ, θ_1, θ_2, θ_3	Downwash angle
θ	Angular coordinate
ρ	Air density
Λ	Sweep-back angle of wing quarter-chord line
ω	Vorticity defined in equation (4.16)
ψ	Stream function defined in equation (4.14)
ξ	Dummy variable of integration

STUDIES ON THE INTERFERENCE OF WINGS AND PROPELLER SLIPSTREAMS

By

Ramadas K. Prabhu[1] and Surendra N. Tiwari[2]

SUMMARY

The small disturbance potential flow theory is applied to determine the lift of an airfoil in a nonuniform parallel stream. The given stream is replaced by an equivalent stream with a certain number of velocity discontinuities, and the influence of these discontinuities is obtained by the method of images. Next, this method is extended to the problem of an airfoil in a nonuniform stream of smooth velocity profile. This model allows perturbation velocity potential in a rotational undisturbed stream. A comparison of these results with numerical solutions of Euler equations indicates that, although approximate, the present method provides useful information about the interaction problem while avoiding the need to solve the Euler equations.

The assumptions of the classical lifting line theory applied to the wing-slipstream interaction problem are scrutinized. One of the assumptions (uniform velocity in the slipstream) of the classical theory is dropped, and the governing equations are derived for the spanwise lift distribution on a wing in a single axisymmetric slipstream. Spanwise lift and induced drag distributions are obtained for two typical cases, and the effects of nonuniformity in the slipstream

[1]Graduate Research Assistant, Deparment of Mechanical Engineering and Mechanics, Old Dominion University, Norfolk, Virginia 23508.

[2]Eminent Professor, Department of Mechanical Engineering and Mechanics, Old Dominion University, Norfolk, Virginia 23508.

velocity profile are examined.

The method of matched asymptotic expansions is applied to the problem of a large aspect ratio swept wing in the slipstream of multiple overlapping propellers. The flow is assumed to be steady, inviscid and incompressible. It is also assumed that the height of the slipstream is of the order of the wing chord, and its spanwise extent is of the order of the wing span. Three different flow regions are identified by employing different stretching transformations, and asymptotic expansions are introduced using the chord-to-span ratio as the small expansion parameter. The details of the nonuniform flow in the slipstream enter into the wing-sectional analysis. In the outer limit, the wing shrinks to a swept lifting line, and the slipstream reduces to a thin sheet of jet carrying the momentum gain from the propeller. The curvature of this jet sheet results in a pressure difference which is represented by a vortex sheet. The governing equations are solved by discretization. Comparison of the present results with the experimental data as well as other numerical solutions showed generally good agreement.

Chapter 1

INTRODUCTION

The cost of aviation fuel has gone up substantially in the last decade and this is expected to be an ever increasing trend. Added to this is the uncertainty regarding the supplies. These factors combined with the national concern over energy conservation have lead aircraft designers as well as the operators to give prime importance to fuel efficient propulsion systems for the future aircraft. Prior to the so-called oil crisis in 1973, the fuel cost was a relatively small fraction (about 25 percent) of the direct operating cost, and it was of less concern to the designers/operators. Today, however, it is claimed that this fraction has risen to about 60 percent [1, 2]* , and that it is the major part of the aircraft operating cost.

It was only propellers that provided propulsive force to aircraft before jet engines appeared on the scene. As flight speeds increased, the propellers posed serious problems of rapidly decaying propulsive efficiency and increasing noise and vibration levels. As a result, more powerful and efficient jet engines took over and dominated the scene, and propellers were neglected for many years. It is well known that the old technology propellers are the most efficient mode of propulsion up to a Mach number of about 0.6. The interest generated in the propeller

---

*Numbers in brackets indicate references.

technology since the oil crisis has lead to the development of the prop-fan, which is claimed to operate at an aerodynamic efficiency of about 80 percent at a Mach number of 0.8 [3].

With the prospect of the use of prop-fans on transport airplanes, there has been concern regarding the associated problems. The interference of slipstreams with other parts of the airplane, in particular with the wing, is one of the major problem areas. With the flight speeds going up to M=0.8, compressibility effects can no longer be neglected. The flowfield behind the propeller is highly rotational and the effects of vorticity in the slipstream cannot be ignored. Therefore, the problem in its complete form is quite complex. Consequently, considerable efforts (analytical, numerical and experimental) are being made to understand the rather complex flowfield associated with the wing-slipstream interference.

The problem of determining the influence of the propeller slipstream on the wing lift has been studied quite extensively in the past, and a considerable amount of literature is available. Because of the highly nonuniform nature of the flow in the slipstream, the problem is essentially a nonlinear one; as a result, the work done during the 1930's was based on approximate and semi-empirical methods [4, 5]. These methods provided satisfactory results in the speed-power range for which they were developed. Koning [6] gave an analytical treatment for a wing in a propeller slipstream based on the lifting-line theory. It was assumed in this analysis that the increment in velocity in the slipstream was small. Ferrari [7] developed what is generally referred to as the classical lifting-line theory for wings in slipstreams. The main assumptions in this theory were that (1) the slipstream was in the

form of a circular cylindrical tube extending to infinity both upstream and downstream, (2) the velocity in this tube was uniform (U_J), and (3) the relation between the lift and angle of attack for the wing sections was obtained by considering them to be in uniform flows with velocities U_J and U_∞ for sections inside and outside the slipstream tube, respectively. One of the drawbacks of this theory is the third assumption. It is obvious that the lift produced by an airfoil would depend on the jet height. Ting and Liu [8] employed the method of images and studied the lifting characteristics of thin airfoils in a nonuniform parallel streams. This method can be used to determine the lift of an airfoil in a uniform jet. Chow et al. [9] numerically investigated the two-dimensional nonuniform flow past an airfoil by solving the Euler equations. These results demonstrated the fact that the lift of an airfoil depends not only on the jet height but also on the nonuniformity in the approach stream. Recognizing this fact, Kleinstein and Liu [10] made some improvements to the classical theory. The lift data for the wing sections within the slipstream was obtained by employing the methods of [8] and [9], and was used in the classical theory. However, the assumptions (1) and (2) of the classical theory were still retained while computing the downwash due to trailing vortices. These results demonstrated the effects of modifying the assumption (3) mentioned earlier.

There were other attempts to improve upon the classical theory of Ferrari. Rethorst [11] employed the Weissinger approach and developed a lifting-surface theory. Wu and Talmadge [12], and Cumberbatch [13] extended the method of [11] to wings extending through multiple jets. Jameson [14] modeled wide slipstreams by rectangular and elliptic jets,

and by using the standard imaging technique developed a lifting-surface theory. In all these analyses one of the main assumptions was that the velocity in the jet (representing the slipstream) was uniform.

Ting et al. [15] scrutinized the assumptions of the classical lifting-line theory, and suggested a new approach to solve the problem. It was recognized that the height of the slipstream is of the order of the wing chord, and the spanwise spread of the combined multi-propeller slipstream is of the order of the wing span. Three different flow regions were identified by employing different stretching transformations. Asymptotic expansions were made by using the reciprocal of the wing aspect ratio (1/AR) as the small parameter. This analysis showed that the details of the nonuniform stream enter primarily into the local sectional anlysis; behind the wing, the slipstream acts like a thin jet sheet which supports a pressure difference across itself. By solving the governing integral equation, the wing lift distribution was determined. Maarsingh [16] made an evaluation of this method by comparing these results with the data obtained from some specially designed experiments [17]. Some differences between the two sets of results were found, and these are suspected to be due to inaccuracies in the lift-curve slope data that was used in the computations of Maarsingh [16].

Ribner and Ellis [18] considered slipstreams of arbitrary cross section, and, instead of the standard imaging technique, represented the slipstream boundary by vortex sheaths, and proceeded on the basis of lifting line theory. Lan [19] developed a method based on the quasi-vortex-lattice method and a two-vortex-sheet representation of the slipstream. Both of these methods accounted for the rotation in the

slipstream.

Levinsky, et al. [20, 21] developed a large-tilt-angle lifting-surface theory applicable to tilt-wing and tilt-rotor V/STOL aircraft configurations. An actuator disk analysis for an inclined propeller was developed, and was combined with Weissinger lifting-surface theory for the wing at arbitrary wing angle of attack. Configurations with one, two, or four slipstreams were considered, and effects of slipstream swirl were included in all but single slipstream case. Comparisons with experimental data showed that the theory predicts span loading reasonably well for small angles of attack and small propeller tilt angles.

With the availability of high speed computers and efficient computational techniques, there has been a new trend in the approach to the solution of the wing-slipstream interaction problem. Numerical techniques have been employed to solve the linearized potential flow equations, full potential equations, and Euler equations.

Rizk [22] investigated the propeller slipstream-wing interference problem at transonic speeds. It was noted that a nearly uniform slipstream interacting with a thin wing allows the perturbations to be potential although the undisturbed flow within the slipstream is rotational. The resulting potential flow (boundary value) problem for transonic flow was solved by a finite-difference scheme. In general, however, the assumptions made in this work may not be fully valid; for example, the nonuniformity in the slipstream may be large enough to cause potential flow assumptions to yield erroneous results.

Chandrasekaran and Bartlett [23] modified the Hess panel code to

handle the effects of the propeller slipstream. The slipstream boundary was modeled by a system of ring vortices, and the effects of swirl in the slipstream was included. A comparison of the results with experimental data showed some differences, which were attributed to viscous and compressibility effects as well as to uncertainities in the estimation of the flowfield behind the propeller.

Narain [24] and Samant et al. [25] made assumptions similar to those of Rizk [22] regarding the slipstream, but did not assume that the perturbations were small. Instead, the problem was investigated on the basis of the full potential flow equations with a rigid boundary for the slipstream tube. These results compared reasonably well with available experimental data; however, it should be recognized that the advantage of using the accurate full potential equation is sacrificed by the approximation of irrotational flow.

Whitfield and Jameson [26] solved the three-dimensional Euler equations coupled with the energy equation. The Euler equations had the force terms included to simulate the propeller effects. The viscous effects were accounted for, although approximately, by coupling the three-dimensional Euler equations with the two-dimensional inverse integral boundary-layer equations. In spite of these sophistications, the spanwise lift distribution obtained by this analysis failed to show good agreement consistently with the experimental data of Welge and Crowder [27]. This method, however, provides detailed information on velocity and other flow quantities in the entire computational domain. As may be expected, such an effort would require a large computer memory and a considerable amount of computing time. For example, the computer code developed in [26] required 900,000 words of memory and 341 seconds

of computing time on Cray-1S computer for a relatively coarse (96x16x16) grid.

As a result of this literature survey, it is apparent that there is a need for further research in this field on the following topics:

(1) Airfoil in nonuniform flow

(2) Improvements to lifting line and lifting surface theories

(3) Slipstream swirl and distortion effects

(4) Compressibility and viscous effects

(5) Swept wing - slipstream interference

(6) Interference of slipstream with other parts of the airplane

The main purpose of the present study is to investigate some of these topics. The following paragarphs describe briefly the work undertaken in this study.

As noted earlier, the nonuniformity of the slipstream is not modeled properly in the classical lifting line theory for wing-slipstream interference. This has been improved by using the sectional lift data obtained by either the linearized potential flow method for the wing section in an equivalent jet or the solution of two-dimensional Euler equations. Whereas the assumption of uniform flow for the computation of the sectional lift data in the classical theory is a drastic simplification, employing the Euler equations, although providing the necessary rigor, requires considerable computing effort. Approximating the actual nonuniform velocity profile in the slipstream

by an equivalent uniform jet is a good approximation. However, it is found that better approximations are possible under the framework of the linearized potential flow theory. Chapter 2 includes a study of thin airfoils at small angles of attack in nonuniform parallel streams. These results are compared with numerical solutions of the Euler equations.

It is assumed in the classical lifting-line theory for wing slipstream interference that the slipstream is in the form of a uniform circular jet, for the computation of downwash due to the trailing vortices. The velocity distribution in the slipstream is far from being uniform. However, this approximation (made to simplify the problem) was carried over in the subsequent developments. For example, Kleistein and Liu [10] retained this assumption in their modification of the classical theory, and so did Rethorst and his coworkers [11-13] in the development of the lifting-surface theories. In the present study, the assumption that the velocity in the slipstream is uniform is dropped, and the effects of the nonuniformities in the slipstream on the downwash of a large aspect ratio wing are studied. Chapter 3 includes the lifting-line theory for large aspect ratio wings in slipstreams that can be represented as axisymmetric jets with smooth velocity profiles. Spanwise lift and induced drag distributions are computed for two typical cases. Results are compared with those obtained by other theories.

The asymptotic method has been a powerful tool in the analysis of large aspect ratio wings [28]. The method is simple, and provides a better physical insight into the problem. The asymptotic method has also been used in an analysis of unswept wing-slipstream interference

[15]. An asymptotic method for the analysis of the interference on a large aspect ratio swept wing with multi-propeller slipstream is presented in Chap. 4. It is assumed as in [15] that the height of the slipstream is of the order of the wing chord, and that its width is of the order of the wing span. By employing different stretching transformations, three different regions are identified. Expansions are introduced in each region by using the ratio of the chord to the span as the small parameter. The details of the nonuniformities in the slipstream enter in the two-dimensional flow past wing sections normal to the lifting-line. The spanwise component of the velocity is shown not to affect the sectional lift data. For the outer solution, the wing planform reduces to a swept lifting-line, and the propeller slipstream behind the wing reduces to a thin sheet carrying the sectional momentum gained through the propellers. The curvature of this sheet results in a pressure difference across itself, which is represented by a vortex sheet. The governing equations are solved by a discretization procedure. Several examples are considered for which experimental results are available. Present results are compared with these experimental data as well as other numerical results.

Chapter 2

AIRFOIL IN NONUNIFORM PARALLEL STREAMS

The study of aerodynamic characteristics of lifting surfaces in nonuniform flow is of considerable practical interest. Wing sections behind a propeller experiencing a jet-like velocity profile, and tailplane sections of a conventional airplane experiencing a wake-like velocity profile are two examples of such problems. These problems are complex and require simplifying assumptions. Even if the viscous and compressibility effects are neglected, the presence of vorticity in the approaching stream necessitates the solution of the Euler equations. Being nonlinear, the Euler equations require numerical treatment which has been done by several workers [9,29].

This nonlinear problem can be simplified considerably by replacing the given nonuniform stream by an equivalent uniform jet. The advantage of this approach is the simplification of flow from rotational to irrotational, with a finite number of surfaces of velocity discontinuity. Karman gave the basis for a linearized potential flow analysis of such problems [30]. Glauert employed this method to solve the problem of an airfoil in the presence of a uniform jet [31]. The airfoil was replaced with a single vortex, and the airfoil lift was determined by computing the streamline curvature and increment in axial velocity. Ting and Liu [8] developed a method that is essentially an extension of Glauert's method, which could be used to compute the

chordwise pressure distribution and the lift of a thin airfoil in a uniform jet.

In this chapter the basis for linearized potential flow analysis for the problem of an airfoil near a surface of velocity discontinuity is reviewed. The method of solution of the integral equation of [8] is simplified. The analysis in then extended to cover the case of five streams with four surfaces of discontinuity. Next, the problem of an airfoil in a smooth velocity profile is treated by the linearized potential flow analysis. This problem is also solved by a more rigorous, although more expensive, method by solving the Euler equation using a modified version of the Euler code [29]. Results obtained for two examples by different methods are compared.

2.1 Fundamental Basis for the Analysis

The present linearized potential flow analysis is based on the method due to Karman [30] for representing the flow past a body in the proximity of a surface of velocity discontinuity. Consider two parallel streams with velocities U_0 and U_1, the line AB being the undisturbed streamline separating the two streams (Fig. 2.1). Let a body be placed in the lower stream, and let (u_0, v_0) and (u_1, v_1) be the perturbation velocity components in the lower and the upper streams respectively. If the disturbed streamline separating the two streams makes an angle β with the undisturbed streamline, then

$$\tan\beta = v_0/(U_0 + u_0) = v_1/(U_1 + v_1)$$

Assuming u_0, u_1, v_0 and v_1 to be small compared to U_0 and U_1, transferring this condition to the undisturbed surface, and retaining

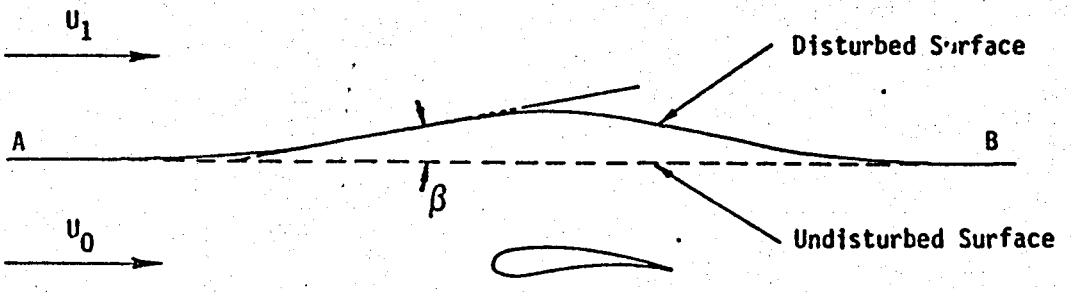

Fig. 2.1 A body near a surface of velocity discontinuity.

only the first order terms, this relation can be simplified to

$$v_0/U_0 = v_1/U_1 \tag{2.1}$$

Also, the static pressure is assumed to be continuous across the surface, i.e.,

$$p_0 - (1/2)\,\rho[U_0^2 - (U_0+u_0)^2 - v_0^2] = p_1 - (1/2)\,\rho[U_1^2 - (U_1+u_1)^2 - v_1^2]$$

where p_0 and p_1 are the static pressures below and above the surface of discontinuity. Retaining only the first order terms, this relation reduces to

$$u_0U_0 = u_1U_1 \tag{2.2}$$

Equations (2.1) and (2.2) are the two necessary conditions that must be satisfied across the undisturbed surface of discontinuity, and form the basis for the analysis in this chapter.

Glauert [31] considered an airfoil near a surface of discontinuity (Fig. 2.2). The airfoil was represented by a vortex of strength Γ. Since the problem is linear, it was demonstrated [31] that application of Eqs. (2.1) and (2.2) lead to a flow in the upper stream as that due to a point vortex of strength $(\Gamma+K)U_1/U_0$ at the point P, and a flow in the lower stream as that due the vortex Γ at P together with its image of strength K at the point P', where

$$K = \Gamma(U_0^2 - U_1^2)/(U_0^2 + U_1^2) = \Gamma\mu$$

A logical extension of this approach is to replace the airfoil by a vortex distribution $\gamma(x)$, $0<x<c$, instead of a single vortex. Each of the vortex elements of this distribution $\gamma(x)dx$ forms images as

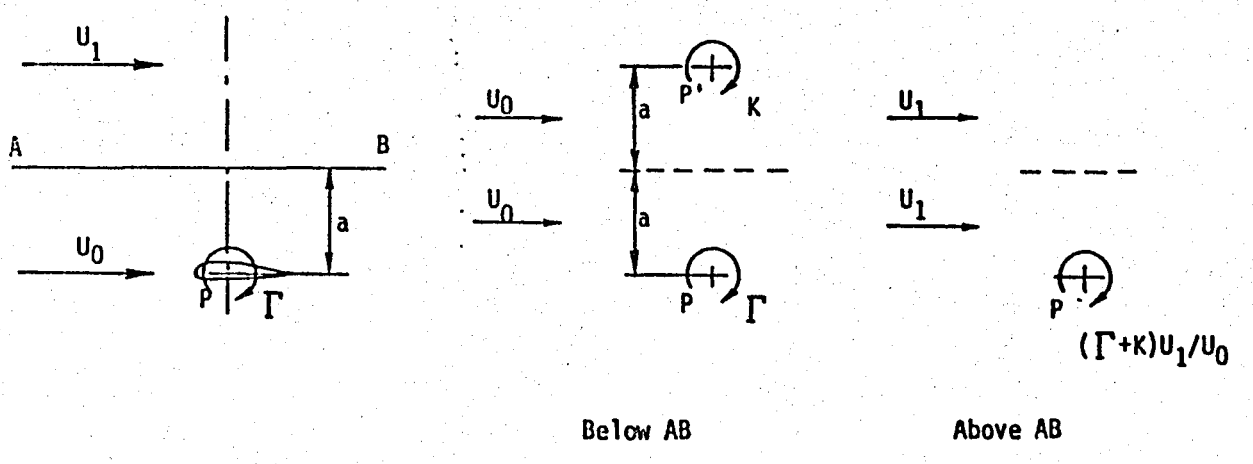

Fig. 2.2 Image system for an airfoil near a surface of velocity discontinuity.

described above. The downwash at the airfoil chord can be determined in terms of $\gamma(x)$ and its image strength $\mu\gamma(x)$, and the unknown $\gamma(x)$ can be determined by satisfying the flow tangency condition on the airfoil mean camber line. This problem can be treated as a particular case of a more general problem of an airfoil in a jet of finite width, which is considered in the following section.

2.2 Airfoil in a Jet of Finite Width

A more interesting problem is the flow past an airfoil placed in a uniform jet of finite width. Consider the general case of three parallel streams of velocities U_1, U_0 and U_{-1} with two surfaces of discontinuity AA and BB separated by a distance h as shown in Fig. 2.3. Let an airfoil of chord c be placed in the middle stream at a distance a below the surface AA. In this case, the conditions (2.1) and (2.2) have to be satisfied at both the surfaces AA and BB. Ting and Liu represented the airfoil by a vortex distribution $\gamma(x)$, $0<x<c$ instead of a single vortex [8]. The conditions (2.1) and (2.2) were applied repeatedly across the surfaces AA and BB, and an infinite set of image vortex distributions (Fig. 2.3) were obtained to describe the flow in the middle stream. The downwash $v(x)$ at a point x on the y-axis due to $\gamma(x)$ and all its images is given by

$$v(x) = \frac{1}{2\pi}\int_0^c \left\{\frac{1}{(x-\xi)} + \sum_{j=0}^{\infty} (\mu\nu)^j \left[\frac{\mu(x-\xi)}{(x-\xi)^2 + 4(jh+a)^2} + \frac{\nu(x-\xi)}{(x-\xi)^2 + 4(jh+b)^2}\right.\right.$$

$$\left.\left. + \frac{2\mu\nu(x-\xi)}{(x-\xi)^2 + 4(J+1)^2h^2}\right]\right\} \gamma(\xi)\, d\xi \qquad (2.3)$$

where

$$\mu = (U_0^2 - U_1^2)/(U_0^2 + U_1^2) \qquad (2.4)$$

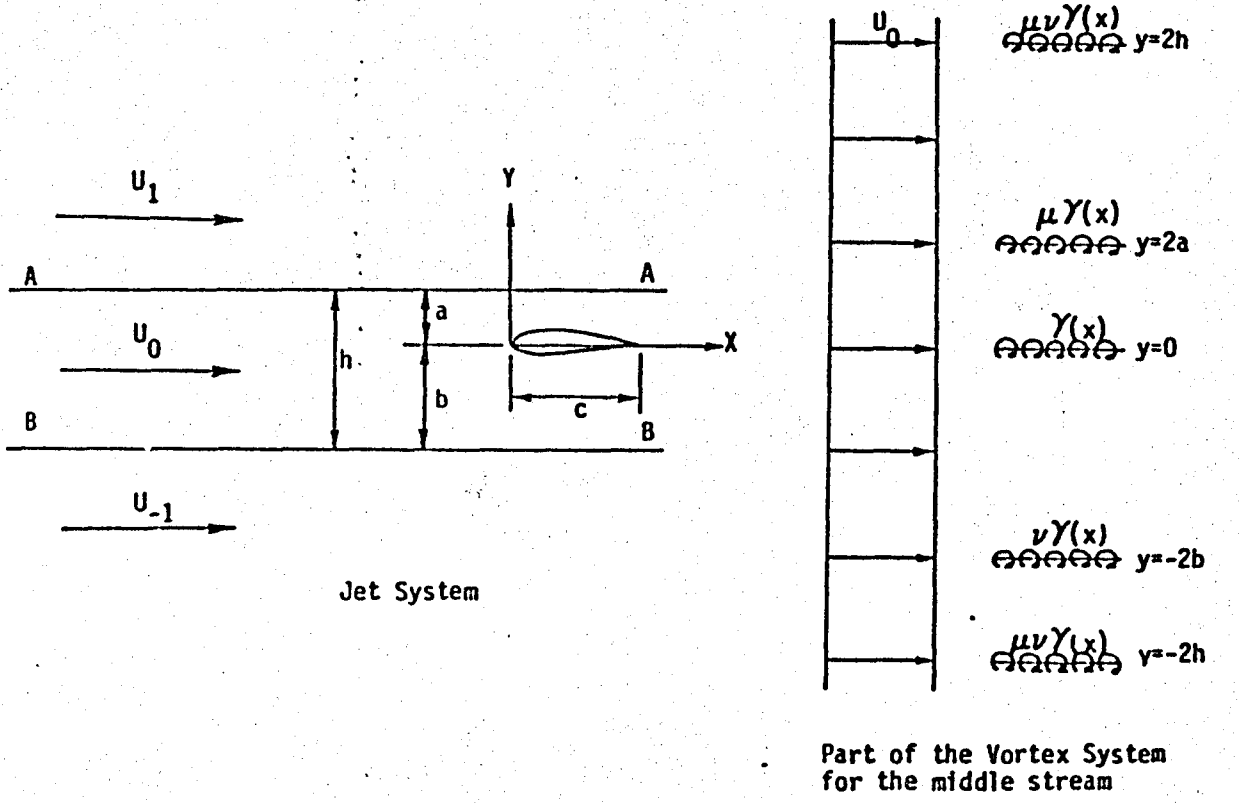

Fig. 2.3 Image system for an airfoil in the middle of three parallel streams.

$$v = (U_0^2 - U_{-1}^2)/(U_0^2 + U_1^2) \qquad (2.5)$$

The linearized flow tangency condition on the airfoil requires

$$v(x) = U_0[\alpha - m(x)] \qquad \text{on } y=0 \qquad (2.6)$$

where α is the angle of attack and $m(x)$ is the slope of the airfoil mean camber line. Equations (2.3) and (2.6) form an integral equation for the unknown $\gamma(x)$. Note that in Eq. (2.3) the first term is the familiar singular term that appears in the classical thin airfoil theory; the other terms are not singular.

The above equation was solved in [8] by employing a rather lengthy procedure. As the integrand in Eq. (2.3) is no more singular than the one in the classical airfoil integral, all the methods of solving the classical integral are applicable in the present case also. In particular, discretization of $\gamma(x)$ is possible. Lan's method of [32] discretizing $\gamma(x)$, and employing a cosine distribution for the vortex and control points is known to produce excellent results for the classical airfoil problem. Hence, this method is used in the present problem.

As the first step towards the solution of Eq. (2.3), x and ξ are replaced by θ and ϕ using the following transformation:

$$x = (1 - \cos\theta)\, c/2 \qquad (2.7a)$$

$$\xi = (1 - \cos\phi)\, c/2 \qquad (2.7b)$$

Then, the Eqs. (2.3) and (2.6) together transform into the following:

$$U_0[\alpha - m(\theta)] = \frac{1}{2\pi}\int_0^{\pi}\left\{\frac{1}{(\cos\phi-\cos\theta)} + \sum_{k=0}^{\infty}(\mu\nu)^j\left[\frac{\mu(\cos\phi-\cos\theta)}{(\cos\phi-\cos\theta)^2 + 16(jh+a)^2/c^2}\right.\right.$$

$$+\frac{\nu(\cos\phi-\cos\theta)}{(\cos\phi-\cos\theta)^2+16(jh+b)^2/c^2}+\frac{2\mu\nu(\cos\phi-\cos\theta)}{(\cos\phi-\cos\theta)^2+16(j+1)^2h^2/c^2}]]\ \gamma(\phi)\ d\phi \tag{2.8}$$

Next, the vortex points and the control points are chosen as follows:

$$\phi_k = (2k-1)\pi/2N, \qquad k=1,2,\ldots,N \tag{2.9}$$

$$\theta_i = i\pi/N, \qquad i=1,2,\ldots,N \tag{2.10}$$

With this, Eq. (2.8) reduces to

$$U_0[\alpha - m(\theta_i)] = \frac{1}{2N}\sum_{k=1}^{N}\{\frac{1}{(\cos\phi_k-\cos\theta_i)}$$

$$+\sum_{j=0}^{\infty}(\mu\nu)^j[\frac{\mu(\cos\phi_k-\cos\theta_i)}{(\cos\phi_k-\cos\theta_i)^2+16(jh+a)^2/c^2}+\frac{\nu(\cos\phi_k-\cos\theta_i)}{(\cos\phi_k-\cos\theta_i)^2+16(jh+b)^2/c^2}$$

$$+\frac{2\mu\nu(\cos\phi_k-\cos\theta_i)}{(\cos\phi_k-\cos\theta_i)^2+16(j+1)^2h^2/c^2}]]\ \gamma(\phi_k)\ \sin\phi_k, \quad i=1,2,\ldots,N \tag{2.11}$$

This is a set of linear simultaneous equations for the unknowns $\gamma(\phi_k)$, $k=1,2,\ldots,N$, and can be solved easily. The lift and pitching moment coefficients of the airfoil are given by

$$c_\ell = (\pi/N)\sum_{k=1}^{N}\gamma(\phi_k)\sin\phi_k \tag{2.12}$$

$$c_m = -(\pi/2N)\sum_{k=1}^{N}\gamma(\phi_k)\sin\phi_k(1-\cos\phi_k) \tag{2.13}$$

Note that the series with index j in Eq. (2.11) converges fast, and hence can be truncated. It has been found sufficient to take N=15 and obtain good accuracy for the $\gamma(x)$ distribution.

2.3 Airfoil in the Middle of Five Streams

Consider the problem of an airfoil in the presence of an infinite series of jets of the same width h. Let the velocity in the nth jet be denoted by U_n, $-\infty<n<+\infty$. Let an airfoil be located in the middle of the principle jet in which the velocity is U_0. If the airfoil is represented by a vortex of circulation Γ, then the flow in any jet can be described by an infinite series of equispaced point vortices at the centers of each jet. The strength of these image vortices for the nth jet is denoted by K(n,s), $-\infty<s<+\infty$. In general, the following relation is true:

$$K(n,n) = 0, \qquad n \neq 0 \tag{2.14}$$

$$K(0,0) = \Gamma \tag{2.15}$$

By applying conditions (2.1) and (2.2) at the surface of discontinuity between the nth and (n+1)th jets, the following recurrence relation can be obtained for the strength of vortices:

$$\beta_{n+1}\, K(n+1,n+s+1) = K(n,n+s+1) - \alpha_{n+1}\, K(n,n-s), \qquad \begin{matrix}-\infty<n<\infty \\ -\infty<s<\infty\end{matrix} \tag{2.16}$$

where

$$\alpha_n = (U_n^2-U_{n+1}^2)/(U_n^2+U_{n+1}^2) \tag{2.17a}$$

$$\beta_n = \sqrt{(1-\alpha_n^2)} \tag{2.17b}$$

Equation (2.16) can be solved in principle; but as pointed out by Glauert the solution is extremely complex [31]. If, however, only five streams are considered as shown in Fig. 2.4, then the problem is simplified to some extent. When the conditions (2.1) and (2.2) are

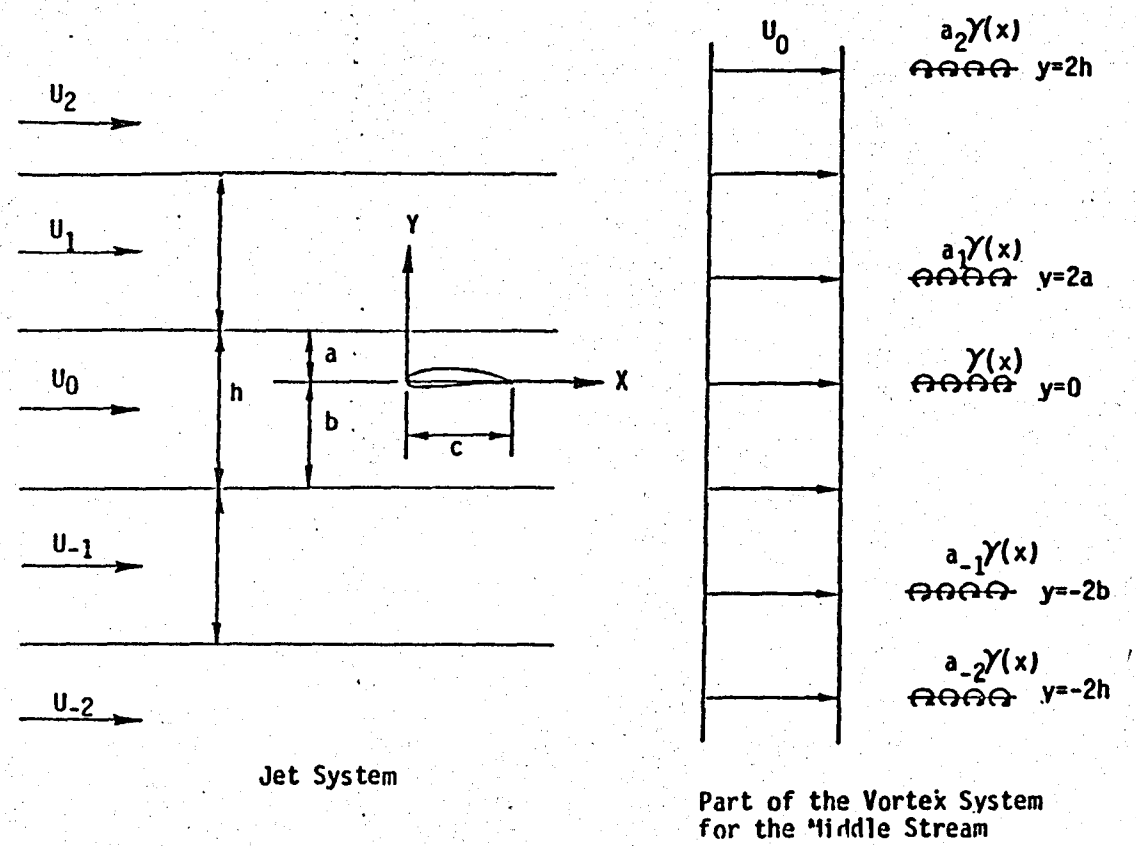

Fig. 2.4 Image system for an airfoil in the middle of five parallel streams.

applied to the four surfaces of discontinuity, four relations similar to Eq. (2.16) are obtained with n assuming the values 2,1,0 and -1 only. Denoting K(2,s), K(1,s), K(0,s), K(-1,s) and K(-2,s) by I_s, J_s, Γ_s, K_s and L_s respectively, Eq. (2.16) can be written for the four different values of n as follows:

$$\beta_2 I_{s+2} = J_{s+2} - \alpha_2 J_{1-s} \tag{2.18a}$$

$$\beta_1 J_{s+1} = \Gamma_{s+1} - \alpha_1 \Gamma_{-s} \tag{2.18b}$$

$$\beta_0 \Gamma_s = K_s - \alpha_0 K_{-s-1} \tag{2.18c}$$

$$\beta_{-1} K_{s-1} = L_{s-1} - \alpha_{-1} L_{-s-2} \tag{2.18b}$$

where $I_s = 0$ for $s > 2$,

$J_1 = 0$, $\Gamma_0 = \Gamma$, $K_{-1} = 0$

$L_s = 0$ for $s < -2$

The solution of the set of Eq. (2.18) can be obtained by substituting successively positive and negative values for s. However, with some algebraic manipulations, it is possible to obtain the following recurrence relations for Γ_s:

$$\Gamma_s = \alpha_1 \Gamma_{1-s} + \alpha_2 \Gamma_{3-s} - \alpha_1 \alpha_2 \Gamma_{s-2}, \qquad s > 2, \tag{2.19a}$$

$$\Gamma_s = -\alpha_0 \Gamma_{-1-s} - \alpha_{-1} \Gamma_{-3-s} - \alpha_0 \alpha_{-1} \Gamma_{s+2}, \qquad s < -2, \tag{2.19b}$$

$\Gamma_0 = \Gamma$, $\Gamma_1 = \alpha_1 \Gamma$, and $\Gamma_{-1} = -\alpha_0 \Gamma$

Some of the values of Γ_s computed using these relations are given below:

$$\Gamma_2 = -\alpha_0\alpha_{-1}\Gamma = \Gamma_{-2}$$

$$\Gamma_3 = (\alpha_2\beta_1^2 - \alpha_0\alpha_1^2)\Gamma$$

$$\Gamma_{-3} = (\alpha_0^2\alpha_1 - \alpha_{-1}\beta_0^2)\Gamma \quad .$$

$$\Gamma_4 = (\alpha_0^2\alpha_1^2 - \alpha_0\alpha_2\beta_1^2 - \alpha_1\alpha_{-1}\beta_0^2)\Gamma = \Gamma_{-4}, \text{ etc.}$$

In general $\Gamma_n = a_n\Gamma$, $-\infty<n<\infty$ where a_n's are constants that depend only on $U_2,\ldots,U_{-2}$. Now, following the procedure adopted in the previous section the airfoil is replaced by a vortex distribution $\gamma(x)$, $0<x<c$ instead of a single vortex. Then the images will also be vortex distributions $a_n\gamma(x)$. Note that it is not necessary to place the airfoil in the middle of the central jet. The image system for the primary stream, when the airfoil is offset from the centerline is shown in Fig. 2.4. The downwash induced by the distribution $\gamma(x)$ and all its images, at a point x on the y-axis is given by

$$v(x) = \frac{1}{2\pi}\int_0^c \left\{ \frac{1}{(x-\xi)} + \sum_{n=-\infty}^{\infty} \frac{a_{2n+1}(x-\xi)}{(x-\xi)^2 + 4(nh+a)^2} + \sum_{\substack{n=-\infty \\ n\neq 0}}^{\infty} \frac{a_{2n}(x-\xi)}{(x-\xi)^2 + 4n^2h^2} \right\}\gamma(\xi)\, d\xi \qquad (2.20)$$

This is the required expression for the downwash at a station x on the y-axis. The unknown $\gamma(x)$ in Eq. (2.20) is determined by employing the flow tangency condition at the mean camber line.

As the first step in the solution, x and ξ are transformed into θ and ϕ respectively as in Eq. (2.7). With these, Eq. (2.20) is transformed into the following:

$$v(\theta) = \frac{1}{2\pi}\int_0^{\pi}\left\{\frac{1}{(\cos\phi-\cos\theta)} + \sum_{n=-\infty}^{\infty}\frac{a_{2n+1}(\cos\phi-\cos\theta)}{(\cos\phi-\cos\theta)^2 + 16(nh+a)^2/c^2}\right.$$

$$\left. + \sum_{\substack{n=-\infty \\ n\neq 0}}^{\infty}\frac{a_{2n}(\cos\phi-\cos\theta)}{(\cos\phi-\cos\theta)^2 + 16n^2h^2/c^2}\right\}\gamma(\phi)\,\sin\phi\,d\phi \qquad (2.21)$$

On discretizing $\gamma(\phi)$ and choosing ϕ_k and θ_i as the vortex points and control points respectively as in Eqs. (2.9) and (2.10), the integral in Eq. (2.21) can be replaced by a finite sum

$$v(\theta_i) = \frac{1}{2N}\sum_{k=1}^{N}\left\{\frac{1}{(\cos\phi_k-\cos\theta_i)} + \sum_{n=-\infty}^{\infty}\frac{a_{2n+1}(\cos\phi_k-\cos\theta_i)}{(\cos\phi_k-\cos\theta_i)^2 + 16(nh+a)^2/c^2}\right.$$

$$\left. + \sum_{\substack{n=-\infty \\ n\neq 0}}^{\infty}\frac{a_{2n}(\cos\phi_k-\cos\theta_i)}{(\cos\phi_k-\cos\theta_i)^2 + 16n^2h^2/c^2}\right\}\gamma(\phi_k)\,\sin\phi_k, \quad i=1,2,\ldots,N \qquad (2.22)$$

The linearized flow tangency boundary condition on the y-axis at the control points requires

$$v(\theta_i) = U_0[\alpha - m(\theta_i)], \quad i = 1,2,\ldots,N \qquad (2.23)$$

The resulting set of simultaneous equations can be solved for the unknowns $\gamma(\phi_k)$, k=1,2,...,N. The lift and the pitching moment of the airfoil can be computed using the relations (2.12) and (2.13) respectively.

Although the summation in Eq. (2.22) goes from $-\infty$ to $+\infty$, it is sufficient to take only a few terms. This is because the image vortices at greater distances from the airfoil are weaker and contribute very little to the downwash. It is found that about 15 terms in the summation are sufficient to provide better than 0.1 percent accurate results.

The two problems considered earlier, namely an airfoil near a surface of velocity discontinuity (Sec. 2.1), and an airfoil in a jet of finite width (Sec. 2.2), can be obtained as special cases of the present problem. For example, if $U_2 = U_1$ and $U_0 = U_{-1} = U_{-2}$, then the problem considered in Sec. 2.1 is obtained, whereas if $U_2 = U_1$ and $U_{-2} = U_{-1}$, then the problem considered in Sec. 2.2 is obtained. Thus a single computer program (meant to solve the present problem) can be used to obtain the results for all the cases considered so far.

2.4 Airfoil in a Stream of Smooth Velocity Profile

So far the problem of an aifoil in a stream with a finite number (one, two, or four) of surfaces of velocity discontinuity was considered. This analysis can in principle be extended to the case of an undisturbed stream with a large number of velocity discontinuities. The solution of this problem would be, as pointed out earlier, rather complex. However, if the changes in the velocities in adjacent small-width streams are small, then an elegant solution can be obtained. This approach can be used to solve for the pressure distribution on an airfoil in a stream of smooth nonuniform profile.

Consider, as in the previous section, a large number of jets each of the same width h, the uniform velocity in the nth jet being denoted by U_n. Let the airfoil be placed on the axis of a jet in which the velocity is U_0 (Fig. 2.5), and let the airfoil be represented by a vortex Γ. The discontinuity surfaces cause image vortices to be formed. The strength of these image vortices is governed by Eq. (2.16). It is assumed that the variation of velocity in adjacent jets is small, i.e., $(U_{n+1} - U_n) = u_n \ll U_n$, for all n. In this case the

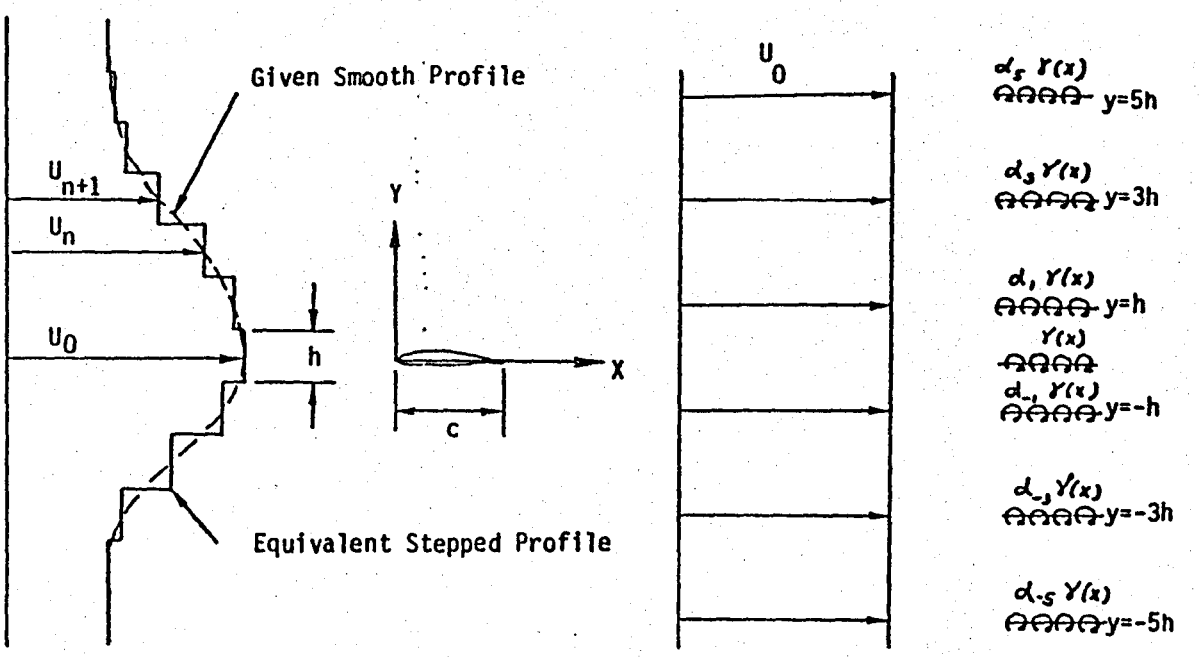

Fig. 2.5 Image system for an airfoil in a stream of stepped velocity profile.

expression for α_n reduces to the following simple form:

$$\alpha_n = \frac{U_n^2 - U_{n+1}^2}{U_n^2 + U_{n+1}^2} = -\frac{2U_n u_n + u_n^2}{2U_n^2 + 2U_n u_n + u_n^2} \approx -\frac{u_n}{U_n} \qquad \text{for } u_n \ll U_n \qquad (2.24)$$

With $|\alpha_n| \ll 1$, a first order solution can be obtained for Eq. (2.16). The resulting image system for the primary jet is found to be following:

$$\Gamma_0 = \Gamma \qquad \text{at } y=0 \qquad (2.25a)$$

$$\Gamma_{2n} = 0 \qquad (2.25b)$$

$$\Gamma_{2n+1} = \alpha_n \Gamma \qquad \text{at } y = (2n+1)h \quad n > 0 \qquad (2.25c)$$

$$= -\alpha_n \Gamma \qquad \text{at } y = (2n+1)h \quad n \leq -1 \qquad (2.25d)$$

If the airfoil is represented by a vortex distribution $\gamma(x)$ instead of a single vortex Γ, then the image system would be very similar (Fig. 2.5). The downwash at a point x on the airfoil due to $\gamma(x)$ and all its images is given by

$$v(x) = \frac{1}{2\pi} \int_0^c \left\{ \frac{1}{(x-\xi)} + \sum_{n=0}^{\infty} \frac{\alpha_n (x-\xi)}{(x-\xi)^2 + (2n+1)^2 h^2} - \sum_{n=-1}^{-\infty} \frac{\alpha_n (x-\xi)}{(x-\xi)^2 + (2n+1)^2 h^2} \right\} \gamma(\xi)\, d\xi \qquad (2.26)$$

Note that α_n's are defined in Eq. (2.24). For a given (thin) airfoil at a (small) angle of attack, the slope of the mean camber line is known, and as in the previous section, the unknown vortex distribution $\gamma(x)$ is determined by satisfying the linearized flow tangency boundary condition

on the y-axis. Note that in deriving Eq. (2.26), it was assumed that the differences in velocities in adjacent jets are small.

Analysis of an airfoil in an infinite series of jets is of little practical interest. However, when the differences in velocities in adjacent small-width jets are small, the velocity profile may be considered as an approximation to a nonuniform smooth velocity profile. It is possible to formally extend the present analysis to the case of an undisturbed stream of a smooth velocity profile by reducing the width (h) and correspondingly increasing the number of jets. For small h (=dy), u = (dU/dy)dy, the expression for α_n reduces to

$$\alpha_n = -\frac{1}{U}\frac{dU}{dy}\,dy \tag{2.27}$$

where U and dU/dy are measured at (2n-1)h/2 = ndy - dy/2. The corresponding image is located at (2n-1)h = 2ndy - dy. In the limit as h tends to zero, the summations in the integrand in Eq. (2.26) are replaced by the corresponding integrals. With this, the downwash Eq. (2.26) can be rewritten as

$$v(x) = \frac{1}{2\pi}\int_0^c \left\{ \frac{1}{(x-\xi)} - \int_0^\infty \frac{1}{U}\frac{dU}{dy}\frac{(x-\xi)\,dy}{(x-\xi)^2 + 4y^2} + \int_{-\infty}^0 \frac{1}{U}\frac{dU}{dy}\frac{(x-\xi)\,dy}{(x-\xi)^2 + 4y^2} \right\} \gamma(\xi)\,d\xi \tag{2.28}$$

If the given velocity profile U(y) is even in y, and the airfoil is placed on the line of symmetry, then Eq. (2.26) reduces to the following simpler form:

$$v(x) = \frac{1}{2\pi}\int_0^c \left\{ \frac{1}{(x-\xi)} - 2(x-\xi)\int_0^\infty \frac{1}{U}\frac{dU}{dy}\frac{dy}{(x-\xi)^2 + 4y^2} \right\} \gamma(\xi)\,d\xi \tag{2.29}$$

It can be shown that, for U and dU/dy of the order of unity, the linearized flow tangency boundary condition on y=0 is

$$v(x) = U_0[\alpha - m(x)] \tag{2.30}$$

where $U_0 = U(y=0)$.

For a given smooth velocity profile U(y) with $U(y) \neq 0$, $-\infty<y<\infty$, the integrals within the brackets in Eq. (2.28) or (2.29) can be evaluated using any standard technique and the unknown $\gamma(x)$ can be determined following the method described in Sec. 2.2.

2.5 Results and Discussion

The lifting characteristics of a flat plat airfoil in nonuniform flow are determined using the potential flow approach of Sec. 2.4. Also, the given nonuniform velocity profiles are replaced by equivalent stepped profiles, and the methods of Secs. 2.2 and 2.3 are applied for the computation of the airfoil lift. These results are compared with the numerical solution of the Euler equations.

The lift of a cambered Joukowski airfoil in a nonuniform stream was studied by Chow, et al. [9] and the results are available in [15]. In this example the velocity distribution in the undisturbed stream was assumed to have the following Gaussian profile:

$$U(y)/U_\infty = 1 + a \exp\,[-(y/d)^2] \tag{2.31}$$

where "a" is the maximum excess velocity nondimensionalized using U_∞, and "d" is "a" measure of the spread of the nonuniformity. The value of "d" was chosen as c/1.81 and the value of "a" was varied from zero (uniform flow) to 1.0. The airfoil was placed on the

centerline of this nonuniform stream. As the present method is based on linear analysis, the lift-curve slope computed by this method does not depend on the airfoil camber. Hence for the present potential flow study, the airfoil is replaced by a flat plate.

Figure 2.6 shows the lift-curve-slope of a flat plate (nondimensionalized using the corresponding value in uniform flow) in the nonuniform stream plotted against the parameter "a". The potential solution obtained for the flat plate in (1) equivalent uniform jet (Sec. 2.2), (2) equivalent modified jet (Sec. 2.3), and (3) the given Gaussian velocity jet are also shown in the figure. Also shown in the figure are the results obtained from [15]. One of the observations from this figure is that for a given value of the parameter "a", the potential solution with the uniform jet approximation gives the smallest value of c_{ℓ_α} whereas the given nonuniform jet gives the largest value. The Euler solution gives a value in between these, and it appears that the modified jet approximation gives results closer to the Euler solution.

The available Euler code [29] for uniform flow past an airfoil section was modified so that it could handle a nonuniform approach stream. Using this version of the code, the chordwise pressure distribution and the lift of a NACA 0012 airfoil in a jet of Gaussian velocity profile were computed. The value of the parameter "d" was chosen as 0.5c and the value of "a" was varied. As in the previous example, potential solutions are obtained for a flat plate in (1) equivalent uniform jet, (2) equivalent modified jet, and (3) the given Gaussian velocity jet. All these results are shown in Fig. 2.7. The potential solutions display a behavior observed in the previous example. However, the lift-curve-slopes obtained by the Euler equation

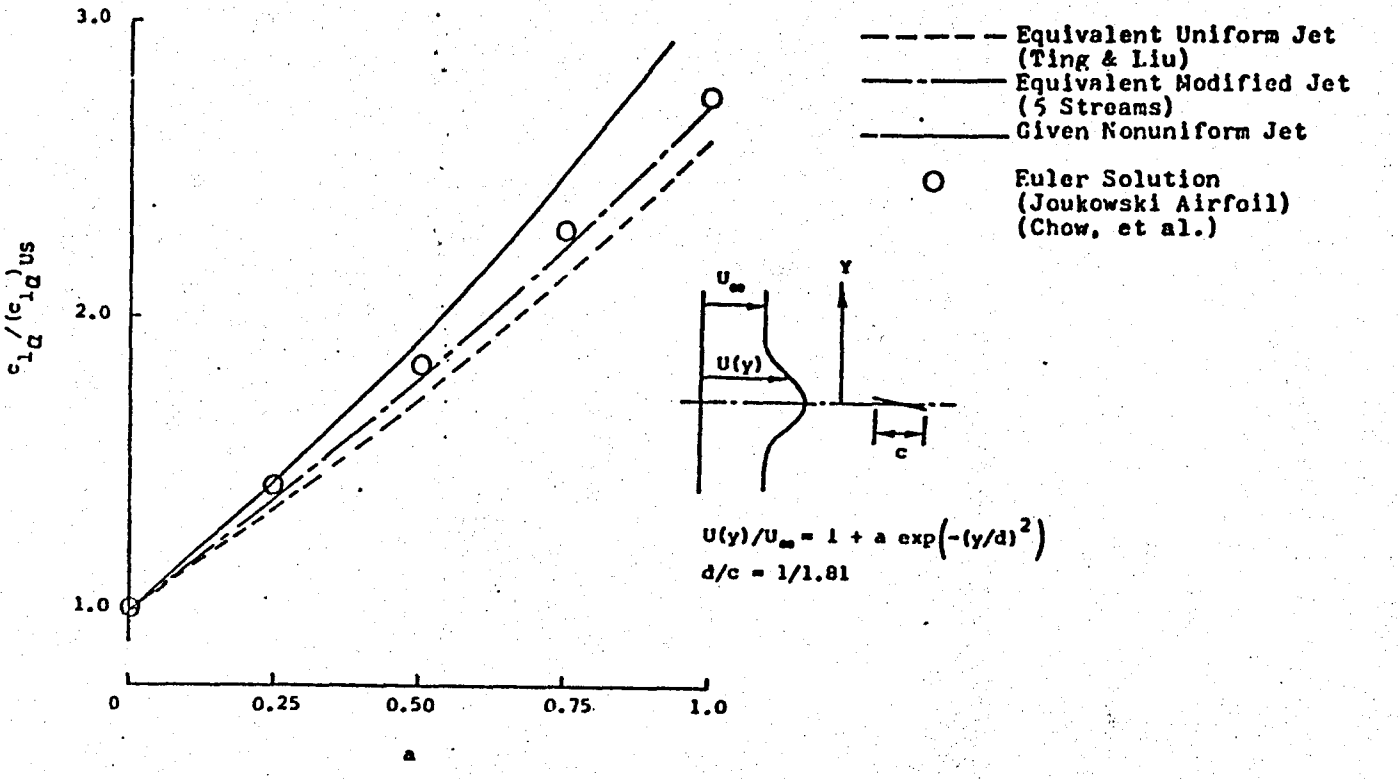

Fig. 2.6 Lift curve slope of a flat plate in a nonuniform flow.

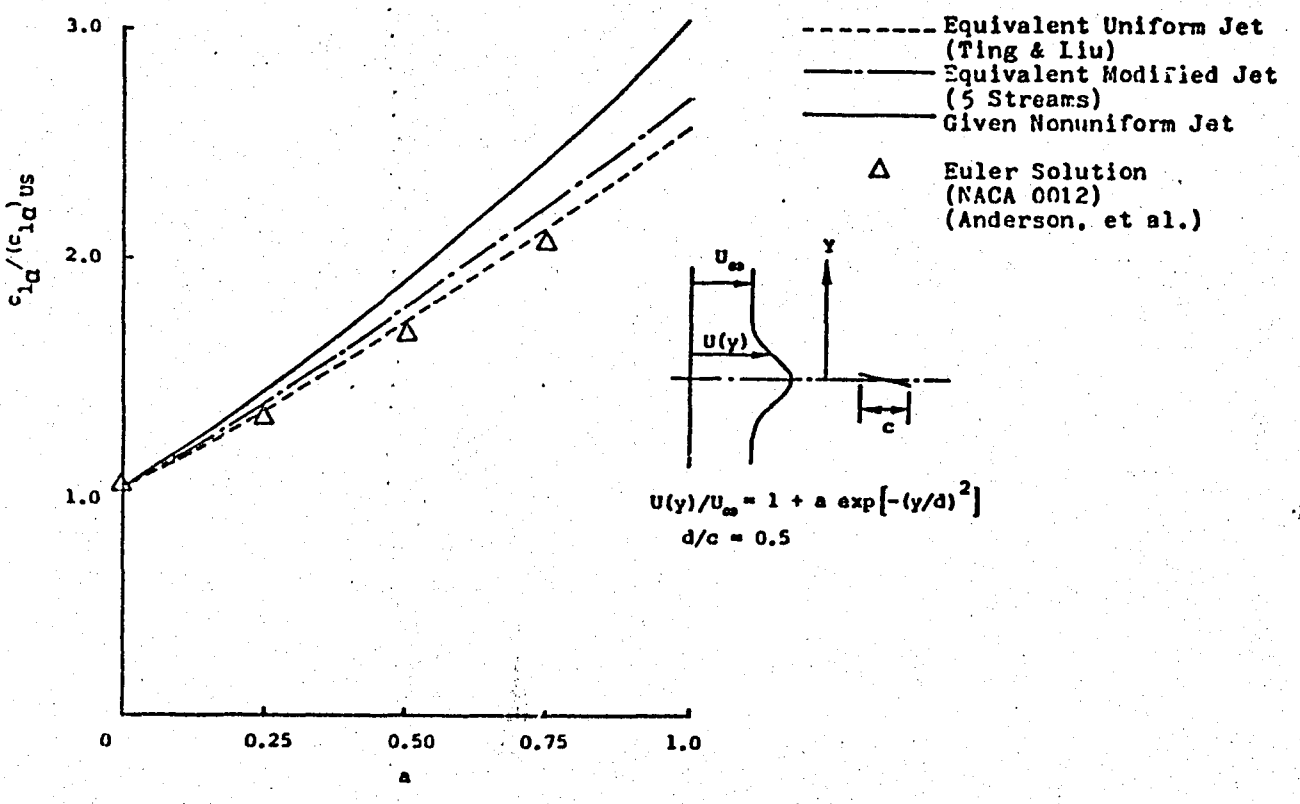

Fig. 2.7 Lift curve slope of a flat plate in a nonuniform flow.

are comparatively smaller than in the previous example.

The chordwise pressure distribution (Δc_p) on the flat plate (obtained by the potential solution) and on the NACA 0012 airfoil (obtained by the Euler solution) at 5-degrees angle of attack are compared in Fig. 2.8. The nonuniform velocity profile is assumed to be Gaussian with a = 0.5 and d/c = 0.5. It may be observed from this figure that there is a reasonably good agreement between the two results.

As the last example, lifting characteristics of a flat plate airfoil in a jet with a modified Gaussian profile are studied. The nonuniform velocity profile is assumed to be the following:

$$U(y)/U_\infty = 1 + a_1 \exp\{-(y^2/d_1^2)\} - a_2 [\exp\{-(y-d_3)^2/d_2^2\} + \exp\{-(y+d_3)^2/d_2^2\}] \qquad (2.32)$$

with $d_1/c = 0.6$, $d_2/c = 0.25$, $d_3/c = 0.155$ and $a_2/a_1 = 0.7$. The factor a_1 serves as the variable.

This velocity profile, sketched in Fig. 2.9, is typical of the axial velocity distribution generally observed behind actual propellers. The maximum velocity occurs not on the centerline but slightly away from it on either side. It is obvious that the approximation of a uniform jet would not be meaningful in the present case. Hence, this approximation is not considered. However, potential solutions were obtained for a flat plate in an equivalent modified jet and in the given nonuniform profile. The results are shown in Fig. 2.9 along with the Euler solution for the NACA 0012 airfoil. It is observed from this figure that in this case the potential solution predicts

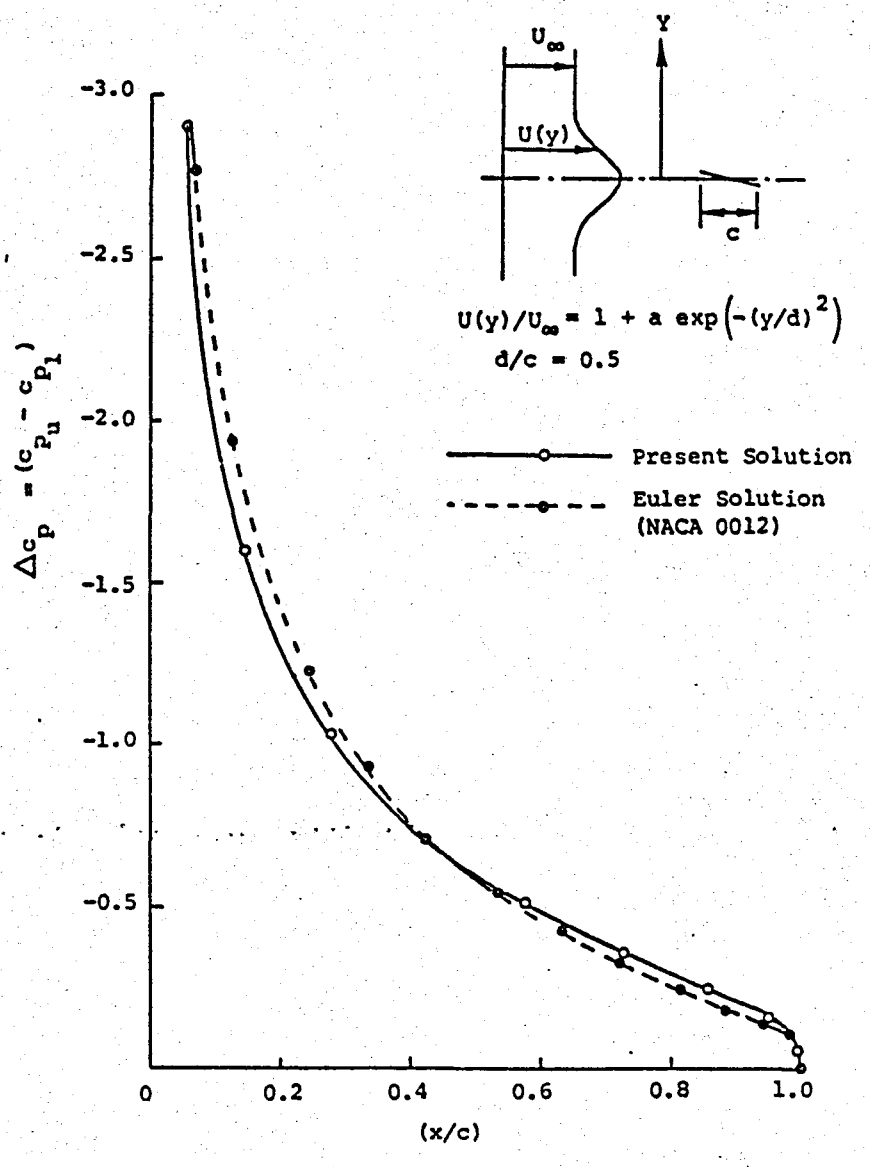

Fig. 2.8 Chordwise pressure distribution on a flat plate in a nonuniform flow.

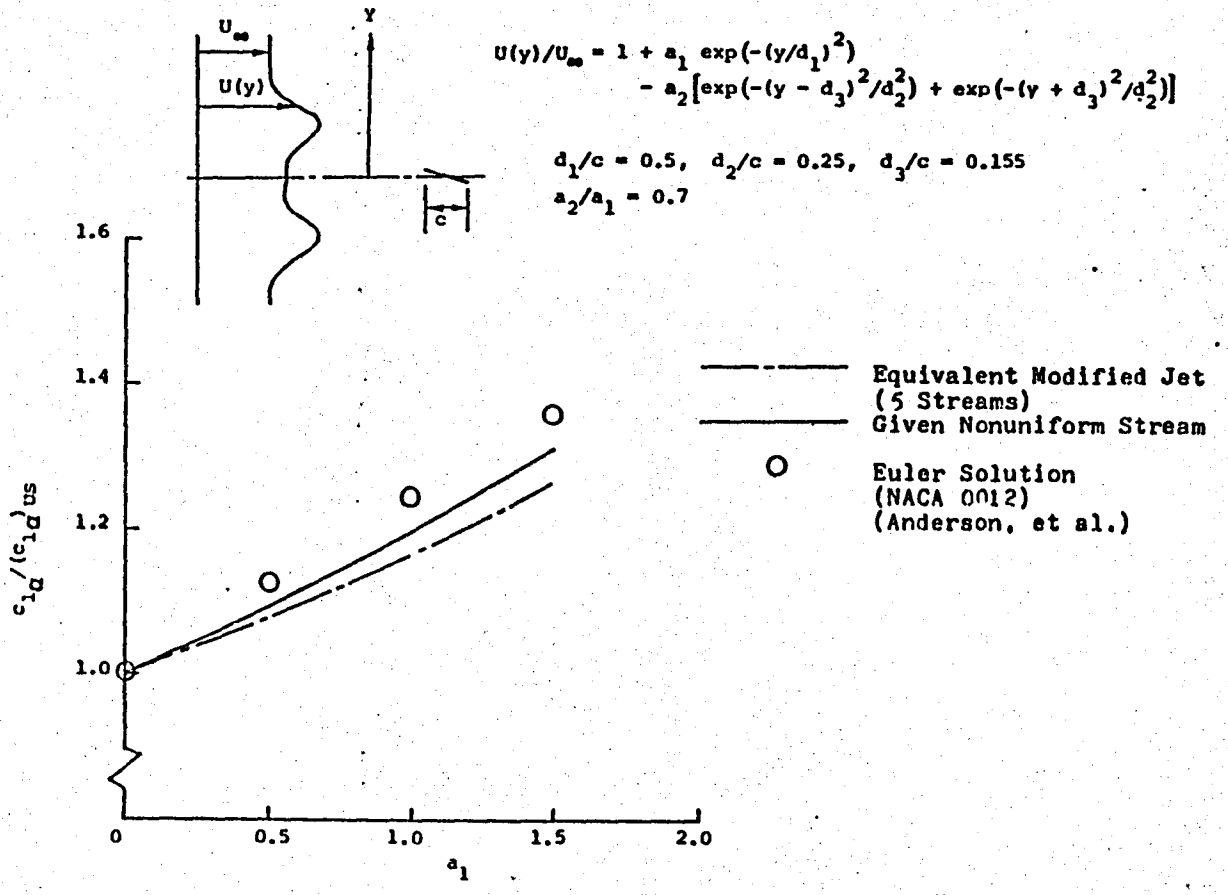

Fig. 2.9 Lift curve slope of a flat plate in a nonuniform flow.

values which are slightly smaller than those obtained by the Euler solutions.

An interesting observation can be made by comparing the results in Figs. 2.7 and 2.9. For the example shown in Fig. 2.7, the Euler solution gave values of c_{ℓ_α} smaller than the corresponding potential solution, but this trend was reversed in the results for the example shown in Fig. 2.9. It was shown by the solution of Euler equations for an airfoil in nonuniform flow [9], that the stagnation streamline comes from a region slightly below the airfoil location. This implies that in the example considered in Fig. 2.7, the airfoil (placed on the centerline of a jet-like Gaussian velocity profile) would have a stagnation streamline with a total pressure slightly lower than the one corresponding to the centerline. Also, this streamline comes from a region having positive vorticity. In contrast, for the example considered in Fig. 2.9, the airfoil (placed on the centerline of a modified Gaussian profile) would experience a stagnation streamline having slightly higher total pressure than the centerline streamline, and coming from a region of negative vorticity. These differences might have contributed to the reversal of the trends observed in Figs. 2.7 and 2.9.

Some differences are observed between the Euler solution and the potential solution. Among several reasons for this, the important one is that the potential solution does not account for the interaction of the vorticity in the undisturbed stream with the airfoil. The effect of the airfoil thickness which is neglected in the potential solution could have contributed to the discrepancy. Yet another factor is the approximations in the numerical solutions of the Euler equations. For

example, in the computer codes [9,29] the perturbations are assumed to be zero on the computational boundary. Considering these factors, the differences between the potential and the Euler solutions do not seem unreasonable.

If the undisturbed stream has a smooth nonuniform velocity profile and an airfoil is placed in it, then the pressure distribution and the lift of the airfoil are to be determined by solving the Euler equations. Being nonlinear these equations are not amenable to analytical study and require numerical treatment. When a small perturbation approximation is introduced, the Euler equations or equivalently the vorticity transport equation reduces to the following linear partial differential equation (written in terms of perturbation velocity components):

$$U(u_y - v_x)x + U_{yy}\, v = 0 \qquad (2.33)$$

where $U = U(y)$ is the undisturbed nonuniform velocity, and $u(x,y)$ and $v(x,y)$ are the perturbation velocity components assumed to be small compared to $U(y)$. Subscripts x and y represent differentiation with respect to x and y, respectively. Since $U(y)$ is assumed to be known, the above equation is a linear partial differential equation with variable coefficients. This equation together with the corresponding continuity equation has to be solved to determine the airfoil lift. The linearized potential flow solution obtained earlier obviously satisfies the equation $(u_y - v_x) = 0$. Hence, it is evident that this solution would also be a solution of the linerized Euler equation only if U_{yy} is small.

The concept of allowing the perturbation velocities to be potential

although the approach stream is rotational is not new. Rizk [20] employed this concept when studying the effects of a slipstream having nonuniform axial and rotational components of velocity on a wing. It was assumed that the undisturbed flow in the slipstream was nearly uniform and that the disturbances due to the wing were small. This lead to a result where the perturbation velocities could be described by a velocity potential. This approach, although approximate, allows obtaining basic information about the interaction problem while avoiding the need to solve the Euler equations. One of the assumptions of the classical lifting-line theory for wings in slipstreams (and some of the related works) is that the propeller slipstream is in the form of a uniform jet. This is a drastic simplification. Although the present analysis does not bring out the interaction of the vorticity in the stream with the airfoil, it is hoped that it would provide a much better approximation than the earlier ones to the actual problem.

Chapter 3

A MODIFIED LIFTING LINE THEORY FOR WING-SLIPSTREAM INTERFERENCE

Consider the problem of determining the lift distribution on a large aspect ratio wing as influenced by a single centrally located propeller slipstream. The classical theory [7] solves this problem making the following three assumptions in addition to those of the classical lifting line theory applied to large aspect ratio wings:

(1) The propeller slipstream is confined within a stream tube of circular cross section in which the velocity is uniform (U_J).

(2) The relation between the sectional lift and angle of attack is the same as that of an airfoil in uniform flow (with velocities U_J and U_∞ for wing sections inside and outside the slipstream respectively).

(3) While computing the downwash, the stream tube representing the slipstream is assumed to extend from upstream infinity to downstream infinity.

Figure 3.1 illustrates these assumptions in some detail. Although the assumption that the propeller slipstream is a stream tube of circular cross section is reasonable, the assumption of uniform velocity within the tube is not realistic. The slipstream behind a propeller has neither a uniform velocity distribution, nor a velocity discontinuity. The second assumption concerning the lift-curve-slope of the wing sections washed by the propeller stream is also not realistic.

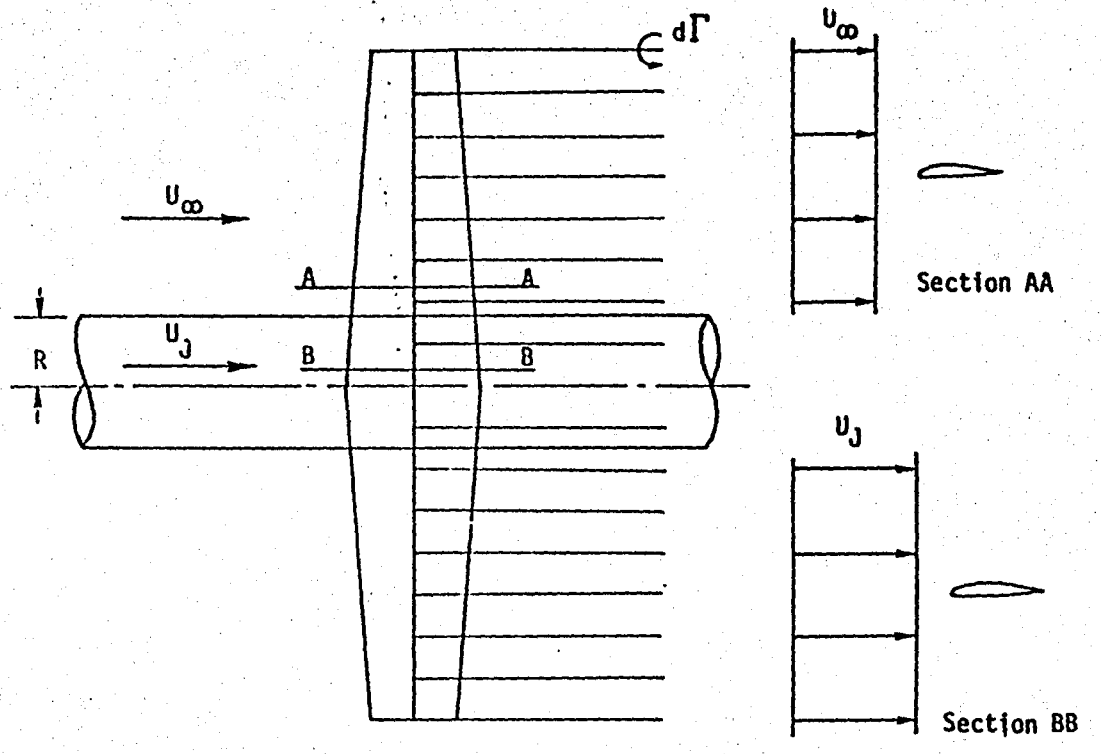

Fig. 3.1 The schematic of the classical analysis.

These rather drastic simplifications of the classical theory prompted several workers to study the problem in detail. Rethorst [11] studied this problem and developed a lifting-surface theory. However, it was assumed that the propeller slipstream was in the form of a uniform circular jet. Kleinstein and Liu [10] scrutinized the assumptions of the classical theory and improved on one of the assumptions. The lift-curve slope of wing sections in the slipstream was computed taking into account the finite width of the slipstream. However, the assumption that the slipstream was in the form of a uniform jet was retained for the computations of the downwash. These results brought out the effects of the assumption (3) above.

In the present analysis the slipstream is assumed to be in the form of an axisymmetric jet with a smooth velocity profile and without a distinct boundary. The relation between the sectional lift and the angle of attack is obtained from a local two-dimensional analysis. For the purpose of computing the downwash due to the trailing vortices, the slipstream is assumed to extend from far upstream to far downstream. With these assumptions, the governing equations are derived for the lift distribution on a wing in slipstream.

3.1 Governing Equations for a Wing in a Single Slipstream

The classical lifting-line theory given by Ferrari [7] for the wing slipstream interaction problem is an extension of Prandtl's lifting-line theory for large aspect ratio wings. The equation governing the spanwise distribution of circulation $\Gamma(y)$ is

$$\Gamma(y) = (1/2)\, U\, c(y)\, c_{\ell_\alpha}(y)\, [\alpha(y) - w(y)/U] \qquad (3.1)$$

where c(y) is the wing chord, $c_{\ell_\alpha}(y)$ is the lift curve slope and $\alpha(y)$ is the angle of attack; also $U=U_J$ for $|y|<R$, i.e., for wing sections inside the slipstream tube and $U=U_\infty$ for $|y|>R$, i.e., for wing sections outside, R being the the slipstream tube radius. The downwash w(y) is given by the relation

$$w(y) = \frac{1}{4\pi}\left\{\int_{-s}^{s}\frac{d\Gamma(\eta)}{(y-\eta)} - \varepsilon_2\left(\int_{-s}^{-R} + \int_{R}^{s}\right)\frac{d\Gamma(\eta)}{(y-\eta)} + \varepsilon_1\int_{-R}^{R}\frac{d\Gamma(\eta)}{(y-R^2/\eta)}\right\}, \quad |y|<R \qquad (3.2a)$$

$$= \frac{1}{4\pi}\left\{\int_{-s}^{s}\frac{d\Gamma(\eta)}{(y-\eta)} - \varepsilon_2\int_{-R}^{R}\frac{d\Gamma(\eta)}{(y-\eta)} - \varepsilon_1\left(\int_{-s}^{-R} + \int_{R}^{s}\right)\frac{d\Gamma(\eta)}{(y-R^2/\eta)}\right\}, \quad |y|>R \qquad (3.2b)$$

where $\varepsilon_1 = (\mu^2-1)/(\mu^2+1)$, $\varepsilon_2 = (\mu-1)^2/(\mu^2+1)$ and $\mu = U_J/U_\infty$. It may be recalled that in deriving these relations, the three assumptions mentioned earlier have been made. Further, when the slipstream is absent, i.e., $U_J = U_\infty$, the factors ε_1 and ε_2 become zero, and Eqs. (3.1) and (3.2) reduce to those of Prandtl's lifting-line theory.

If the jet representing the slipstream has a small excess velocity, i.e., $U_J-U_\infty = u<<U_\infty$, then terms of the order of (u/U_∞) in ε_1 and ε_2 may be neglected. In this case $\varepsilon_1 \approx u/U_\infty$ and $\varepsilon_2 \approx 0$; as a result, Eqs. (3.2a) and (3.2b) are simplified to

$$w(y) = \frac{1}{4\pi}\left\{\int_{-s}^{-s}\frac{d\Gamma(\eta)}{(y-\eta)} + \frac{u}{U_\infty}\int_{-R}^{R}\frac{d\Gamma(\eta)}{(y-R^2/\eta)}\right\}, \quad |y|<R \qquad (3.3a)$$

$$= \frac{1}{4\pi}\left\{\int_{-s}^{s}\frac{d\Gamma(\eta)}{(y-\eta)} - \frac{u}{U_\infty}\left(\int_{-s}^{-R} + \int_{R}^{s}\right)\frac{d\Gamma(\eta)}{(y-R^2/\eta)}\right\}, \quad |y|>R, \qquad (3.3b)$$

Now consider a high aspect ratio wing with the propeller slipstream going past it symmetrically, as shown in Fig. 3.2. Let the undisturbed

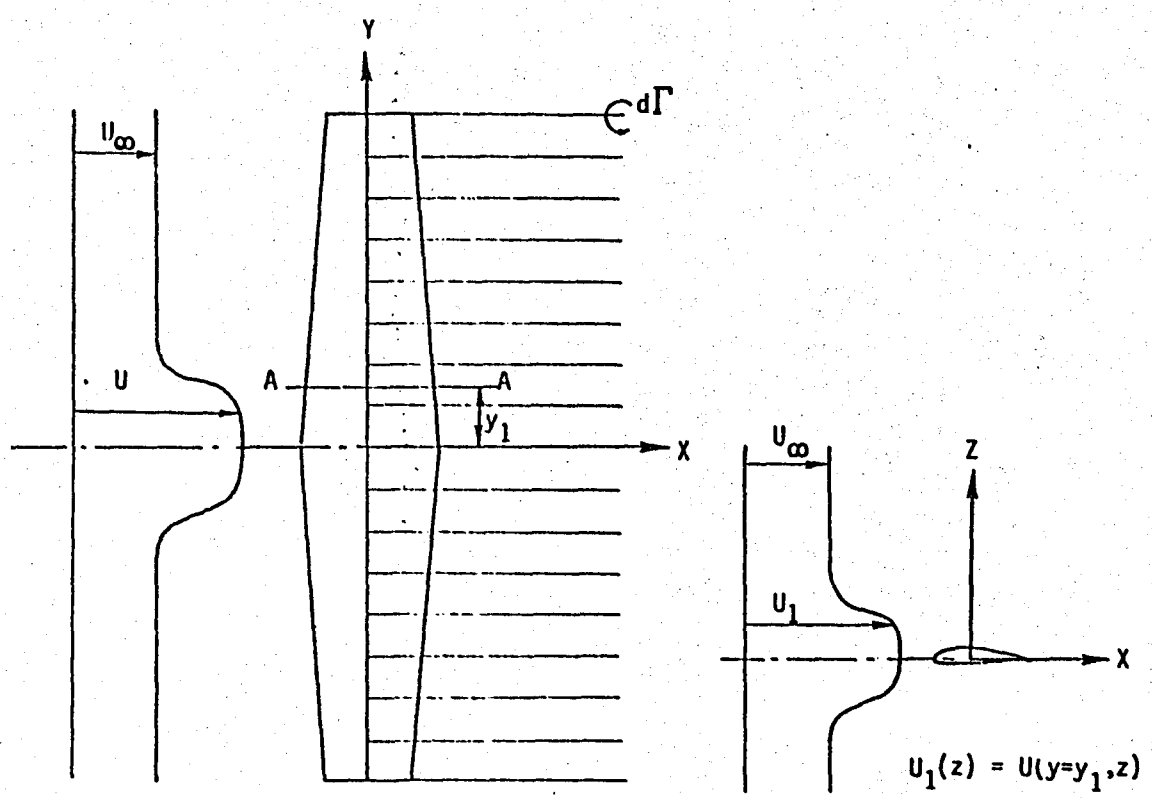

$U = U_\infty[1 + F(r^2)]$

$r^2 = y^2+z^2$, F is a given function.

Section AA

Fig. 3.2 The schematic of the present analysis.

velocity distribution be given by $U(y,z) = U(r) = U_\infty[1+F(r^2)]$ where $r^2 = y^2 + z^2$. Outside the slipstream (i.e., for $r > R$), $F(r^2) = 0$ and $U(y,z) = U_\infty$.

The flowfield inside the slipstream tube is rotational. Nevertheless, it is assumed that the perturbation velocity field due to the wing is irrotational. This concept of potential disturbances in a rotational background flow was employed by Rizk while considering the wing-slipstream interaction problem [22]. The effects of the swirl and compressibility were included and the resulting equations were solved by a numerical technique.

Under the assumption that the disturbances are potential, the lifting-line theory is applicable and the wing is replaced by a lifting line. The circulation $\Gamma(y)$ at a station y on the lifting line is given by

$$\Gamma(y) = (1/2)\, U(y,0)\, c(y)\, c_{\ell_\alpha}(y)\, [\alpha(y) - w(y)/U(y,0)] \qquad (3.4)$$

The lift curve slope $c_{\ell_\alpha}(y)$ is determined by considering the airfoil section in a stream of uniform velocity U_∞ for sections outside the slipstream, and by considering the airfoil section in a stream having a nonuniform velocity profile at the corresponding spanwise station for wing sections within the slipstream. In the present case, the wing section at the spanwise station $y = y_1$ would be in a stream of velocity $U(y=y_1, z)$. The lift curve slope for the wing section in this nonuniform stream is obtained by a two-dimensional analysis. This can be accomplished by solving the Euler equations, which require considerable computational efforts. A simpler, although approximate, method is the linearized potential flow method described in Chap. 2.

For the sake of consistency as well as simplicity the linearized potential flow results are used here.

Before proceeding to determine the downwash w(y) in the present case, it is useful to recall the results in the classical setting, where the velocity within the slipstream tube (a circular section of radius R) is constant. Consider a vortex (representing the wing trailing vortex) of strength γ located at a distance η from the center 0 of the circle representing the slipstream tube (Fig. 3.3). First, consider the case where $|\eta| < R$. By applying the interface conditions of continuity of pressure and streamline slope across the surface of the tube it can be shown [6], that the flow within the circle is described by a vortex of strength γ at η together with its refracted image of strength $(\varepsilon_1 \gamma)$ at the inverse point R^2/η; whereas the flow outside the circle is described by a vortex of strength $(1-\varepsilon_2)\gamma$ at η along with an additional vortex of strength $(\mu\ \varepsilon_1 \gamma)$ at the center of the circle. Similarly, for the case where the vortex is located outside the slipstream boundary (i.e., $|\eta| > R$), it can be shown that the flow within the circle is described by a vortex of strength $(1 - \varepsilon_2)\gamma$ located at η, and the flow outside the circle is described by the vortex γ along with its refracted image of strength $(\varepsilon_1 \gamma)$ located at the inverse point R^2/η, and another vortex of strength $(\varepsilon_1 \gamma)$ at the center of the circle. These results are illustrated in Fig. 3.3.

Now consider a propeller stream with a smooth axisymmetric velocity profile. For the purpose of analysis let this stream be divided into a large number of stepped, concentric annular cylinders of width Δr (Fig. 3.4). Let the axial velocities in the adjacent annular jets with the interface at a radial station r be U and U + u. Consider a vortex of

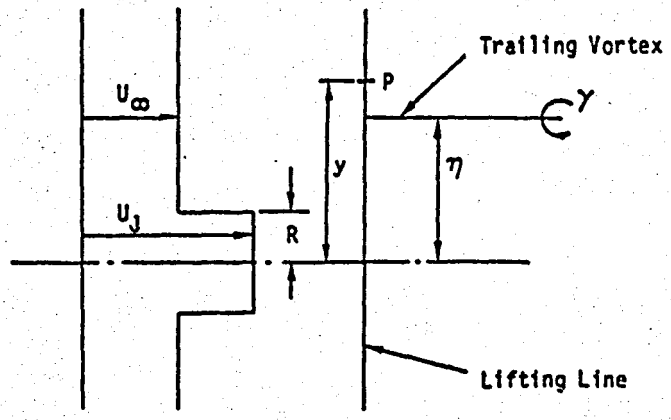

	ACTUAL FLOW	EQUIVALENT FLOW	
		OUTSIDE	INSIDE
VORTEX OUTSIDE	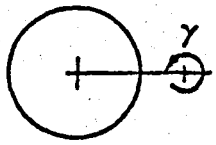	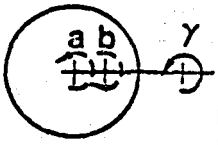	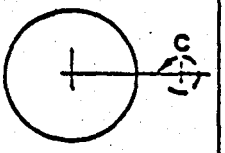
VORTEX INSIDE	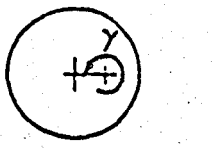	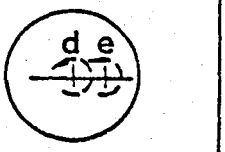	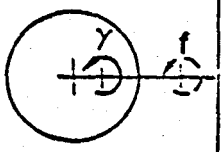

$$a = \epsilon_1\gamma \quad b = \epsilon_1\gamma \quad c = (1-\epsilon_2)\gamma$$

$$d = \mu\epsilon_1\gamma \quad e = (1-\epsilon_2)\gamma \quad f = \epsilon_1\gamma$$

$$\epsilon_1 = (\mu^2-1)/(\mu^2+1) \qquad \epsilon_2 = (\mu-1)^2/(\mu^2+1)$$

$$\mu = \frac{\text{Jet Velocity}}{\text{Outer velocity}}$$

Fig. 3.3 Image system for a uniform jet.

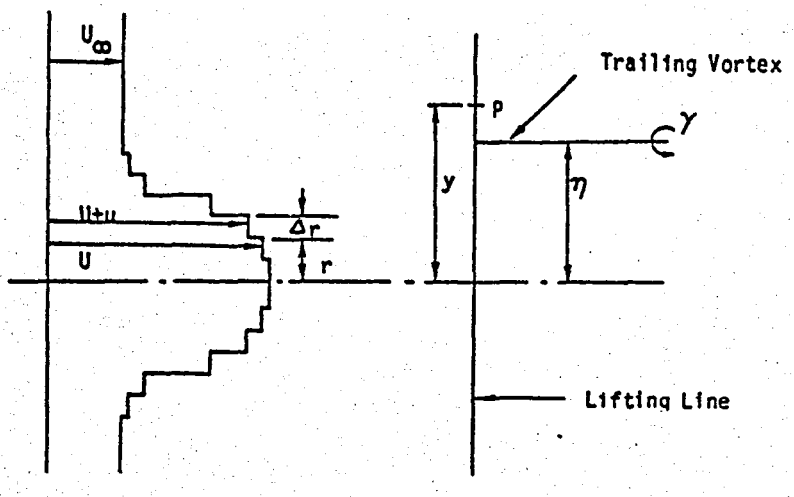

	INNER REGION $\|y\|<R$	OUTER REGION $\|y\|>R$
VORTEX INSIDE $\|\eta\|<R$	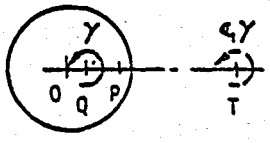	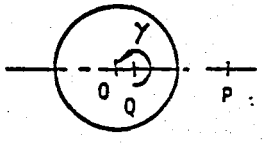
VORTEX OUTSIDE $\|\eta\|>R$	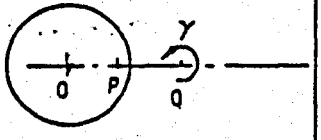	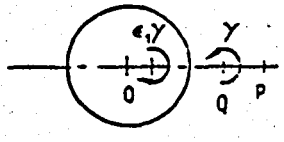

$OP = y_1$; $OQ = \eta$; $OT = R^2/\eta$

Fig. 3.4 Image system for a nonuniform jet.

strength γ located at Q ($OQ = \eta$). It is easy to see that the difference u in the velocities of adjacent jets at the radius r results in an image system as described in the previous paragraph. First consider the case where $|\eta| < r$. It can be shown that the flow in the region $|y| < r$ is described by the vortex at Q with its refracted image of strength $(\epsilon_1\gamma)$ at the inverse point T ($OT = r^2/\eta$), whereas the flow in $|y| > r$ is described by the only vortex at Q. Next, consider the case where $|\eta| < r$. It can be shown that the flow in the region $|y| < r$ is described by the vortex at Q along with its refracted image of strength $(-\epsilon_1\gamma)$ at the inverse point T. These results are illustrated in Fig. 3.4.

The downwash at the spanwise station P ($OP = y$) due to the vortex of strength γ located at Q ($OQ = \eta$) and its image (whenever applicable) resulting from the surface of velocity discontinuity at the radius r is given by

$$\Delta w(y,\eta) = -\frac{\gamma}{4\pi}\left\{\frac{1}{y-\eta} + \frac{\epsilon_1}{y-r^2/\eta}\right\} \qquad |y|<r \qquad (3.5a)$$

$$= -\frac{\gamma}{4\pi}\left\{\frac{1}{y-\eta}\right\} \qquad |y|>r \qquad (3.5b)$$

for the region $|\eta|<r$, and

$$\Delta w(y,\eta) = -\frac{\gamma}{4\pi}\left\{\frac{1}{y-\eta}\right\} \qquad |y|<r \qquad (3.6a)$$

$$= -\frac{\gamma}{4\pi}\left\{\frac{1}{y-\eta} - \frac{\epsilon_1}{y-r^2/\eta}\right\} \qquad |y|>r \qquad (3.6b)$$

for the region $|\eta|>r$. In the limit as Δr tends to zero,

$$u = U(r + \Delta r) - U(r) = (dU/dr)\, dr = U'\, dr$$

so that $$\epsilon_1 = -u/U = -(U'/U)\, dr \qquad (3.7)$$

Letting r to vary from zero to R the following expression is obtained for the downwash at y due to a trailing vortex of strength γ located at η :

$$\Delta w(y,\eta) = -\frac{\gamma}{4\pi}\left\{\frac{1}{y-\eta} + \left[\int_0^{|\eta|} - \int_{|y|}^{R}\right]\frac{U'}{U}\frac{dr}{y-r^2/\eta}\right\}, \quad |y|>|\eta| \qquad (3.8a)$$

$$= -\frac{\gamma}{4\pi}\left\{\frac{1}{y-\eta} + \left[\int_0^{|y|} - \int_{|\eta|}^{R}\right]\frac{U'}{U}\frac{dr}{y-r^2/\eta}\right\}, \quad |y|<|\eta| \qquad (3.8b)$$

If $\Gamma(y)$ is the unknown circulation distribution along the lifting line, then $\gamma = -(d\Gamma(\eta)/d\eta)\, d\eta$. Using this in Eqs. (3.8a) and (3.8b), and integrating from tip to tip the following expression is obtained for the downwash w(y) at the spanwise station y due to the trailing vortices resulting from the distribution $\Gamma(y)$ as influenced by the axisymmetric jet:

$$w(y) = \int_{-s}^{s} \Delta w(y,\eta)\, d\eta$$

$$= \frac{1}{4\pi}\left[\int_{-s}^{s}\frac{d\Gamma(\eta)}{y-\eta} + \left\{\int_{-s}^{-y} + \int_{y}^{s}\right\}\left\{\left(\int_0^{|y|} - \int_{|\eta|}^{R}\right)\frac{U'}{U}\frac{dr}{y-r^2/\eta}\right\} d\Gamma(\eta)\right.$$

$$\left. + \int_{-y}^{y}\left\{\left(\int_0^{|\eta|} - \int_{|y|}^{R}\right)\frac{U'}{U}\frac{dr}{y-r^2/\eta}\right\} d\Gamma(\eta)\right] \qquad (3.9)$$

This equation along with the relation

$$\Gamma(y) = (1/2)\, U(y,0)\, c(y)\, c_{\ell_\alpha}(y)\, [\alpha(y) - w(y)/(U(y,0))] \qquad (3.10)$$

form the required integro-differential equation for the unknown $\Gamma(y)$. For a given wing, $c(y)$ and $\alpha(y)$ are known; in addition, the velocity distribution in the propeller stream $U = U(y,z)$ is assumed known. The sectional lift-curve slope can be determined by the method described in Chap. 2. With these informations, Eqs. (3.9) and (3.10) can be solved for the unknown $\Gamma(y)$. It may be observed at this stage that the effect of the nonuniformity in the slipstream is twofold; it modifies the sectional lift-curve slope as well as the downwash distribution.

3.2 Method of Solution

A simple method of solving the Eqs. (3.9) and (3.10) for the unknown spanwise distribution $\Gamma(y)$ is to assume it to be piecewise constant. This distribution results in a finite number (say N) of trailing vortices. The contribution to downwash from each of these trailing vortices can be computed easily using Eq. (3.8). A summation of these individual contributions over all the N trailing vortices gives the required downwash w.

First, it is convenient to transform y and η into angular coordinates θ and ϕ by using the following transformations:

$$y = s\cos\theta \tag{3.11a}$$

$$\eta = s\cos\phi \tag{3.11b}$$

Next, the trailing vortices are placed at the following N spanwise locations:

$$\phi_k = (2k-1)\pi/2N \qquad k=1,2,\ldots,N \tag{3.12a}$$

The strength of the trailing vortices at these stations are denoted by $\gamma(k)\ 4\pi s\ U_\infty$. The control points are chosen at the following N spanwise locations:

$$\theta_i = i\pi/N \qquad i=1,2,\ldots,N \qquad (3.12b)$$

If Γ_i denote the circulation at the spanwise station $y_i = s\cos\theta_i$, then

$$\Gamma(i) = 4\pi s\ U_\infty \sum_{k=1}^{i} \gamma(k), \quad i=1,2,\ldots,N \qquad (3.13)$$

This expression is used in the discretized version of Eq. (3.10) which is rewritten as

$$4\pi s\ U_\infty \sum_{k=1}^{i} \gamma(k) = (1/2)\ U(i)\ c(i)\ c_{\ell_\alpha}(i)\ [\alpha(i) - w(i)/U(i)], \qquad i=1,2,\ldots,N \qquad (3.14)$$

where $U(i)$, $c(i)$, $c_{\ell_\alpha}(i)$ and $w(i)$ are the velocity in the slipstream, the wing chord, the lift curve slope and the downwash at the spanwise station $y_i = s\cos\theta_i$, respectively. The computation of downwash $w(i)$ is simplified considerably as there are only a finite number (N) of trailing vortices. The contribution to downwash from each of the trailing vortices is given by Eq. (3.8). Hence, the downwash $w_1(i)$ at the control point i due to the N trailing vortices (together with their images) from one side of the wing centerline is obtained by summing the individual contributions. The result is as follows:

$$w_1(i) = U_\infty \sum_{k=1}^{N} \gamma(k) \left\{ \frac{1}{\cos\theta_i - \cos\phi_k} + \left(\int_0^{|\cos\phi_k|} - \int_{|\cos\theta_i|}^{R/s} \right) \frac{U'}{U} \frac{d(r/s)}{\cos\theta_i - (r/s)^2/\cos\theta_k} \right\}, \qquad \text{for } |\cos\phi_k| < |\cos\theta_i| \qquad (3.15a)$$

$$= U_\infty \sum_{k=1}^{N} \gamma(k) \left\{ \frac{1}{\cos\theta_i - \cos\phi_k} + \left(\int_0^{|\cos\theta_i|} - \int_{|\cos\phi_k|}^{R/s} \right) \right.$$

$$\left. \frac{U'}{U} \frac{d(r/s)}{\cos\theta_i - (r/s)^2/\cos\phi_k} \right\}, \qquad \text{for } |\cos\phi_k| > |\cos\theta_i| \qquad (3.15b)$$

This equation can be written symbolically as

$$w_1(i) = U_\infty \sum_{k=1}^{N} G(i,k;U)$$

where

$$G(i,k;U) = \frac{1}{\cos\theta_i - \cos\phi_k} + \left(\int_0^{|\cos\phi_k|} - \int_{|\cos\theta_i|}^{R/s} \right)$$

$$\frac{U'}{U} \frac{d(r/s)}{\cos\theta_i - (r/s)^2/\cos\phi_k}, \qquad \text{for } |\cos\phi_k| < |\cos\theta_i| \qquad (3.16a)$$

$$= \frac{1}{\cos\theta_i - \cos\phi_k} + \left(\int_0^{|\cos\theta_i|} - \int_{|\cos\phi_k|}^{R/s} \right) \frac{U'}{U} \frac{d(r/s)}{\cos\theta_i - (r/s)^2/\cos\phi_k}$$

$$\text{for } |\cos\phi_k| > |\cos\theta_i| \qquad (3.16b)$$

There is a similar contribution to downwash from the trailing vortices on the other half of the wing, so that the total downwash w(i) at the control point i is given by

$$w(i) = U_\infty \sum_{k=1}^{N} \gamma(k) \, [G(i,k;U) - G(i,-k;U)],$$

$$i = 1,2,\ldots,N \qquad (3.17)$$

Upon using this expression for w(i) in Eq. (3.14) the following set of simultaneous equations is obtained for the unknown $\gamma(k)$, k=1,2,...,N:

$$\sum_{k=1}^{i} \gamma(k) \left[1 + \mu(i) \{G(i,k;U) - G(i,-k;U)\}\right]$$

$$+ \sum_{k=i+1}^{N} \gamma(k)\mu(i) \{G(i,k;U) - G(i,-k;U)\} = \mu(i)\, \alpha(i)\, U(i)/U_\infty \qquad (3.18)$$

where $$\mu(i) = c(i)\, c_{\ell_\alpha}(i)\, /8\pi s \qquad (3.19)$$

For a given velocity distribution U(r), the integrals in the function G(i,k;U) can be evaluated using any standard integration method. The lift curve slope $c_{\ell_\alpha}(i)$ of the wing section is computed making a two-dimensional analysis for the nonuniform flow past the wing section at the spanwise station $s\cos\theta_i$. The linearized potential flow method described in Chap. 2 is used for this purpose. With this information all the coefficients in the set of simultaneous equations (3.18) can be determined and the equations can be solved for the unknowns $\gamma(k)$, k=1,2,...,N. Finally the circulation $\Gamma(i)$, lift, and induced drag distribution, and other quantities are computed.

3.3 Results and Discussion

As the first example, a rectangular wing of aspect ratio 6.0 is chosen. The velocity distribution in the slipstream is assumed to have the following Gaussian profile:

$$U(y,z) = U_\infty[1+a \exp\{-(y^2+z^2)/d^2\}] \qquad (3.20)$$

with a = 0.5 and d/s = 0.3. The spanwise lift distribution on the wing

with this slipstream is shown in Fig. 3.5, along with the lift distribution for the wing in the uniform flow for comparison. The figure includes yet another lift distribution on the wing with an equivalent jet of uniform velocity. The velocity and the diameter of this equivalent uniform jet are obtained by equating the mass and momentum in the given slipstream to the corresponding values in the uniform jet. The wing in the given nonuniform slipstream analyzed by the present method produces a C_L = 0.58 whereas for the equivalent uniform jet the C_L = 0.57. Even though the two total lift coefficients are nearly the same, the lift distributions are very different. The present method does bring out the effect of nonuniformity of the velocity distribution in the slipstream on the lift distribution. The induced drag distribution illustrated in Fig. 3.6 also demonstrates this fact.

As the second example, a trapezoidal wing of aspect ratio 6.67 and taper ratio 0.5 is chosen. The velocity distribution in the slipstream is assumed as

$$U(y,z) = U_\infty \left[1+a_1 \exp\{-(y^2 + z^2)/d_1^2\} - a_2 \exp\{-(y^2 + z^2)/d_2^2\}\right] \qquad (3.21)$$

In this modified Gaussian profile, the maximum velocity occurs not on the axis but away from it. With $0<a_2<1+a_1$, this distribution is a better approximation to the velocity distribution in the slipstream of a propeller. In the example chosen a_1 = 0.6, a_2 = 0.75, d_1/s = 0.3, and d_2/s = 0.05. The spanwise lift distribution on the tapered wing with this slipstream is shown in Fig. 3.7. This figure clearly shows the

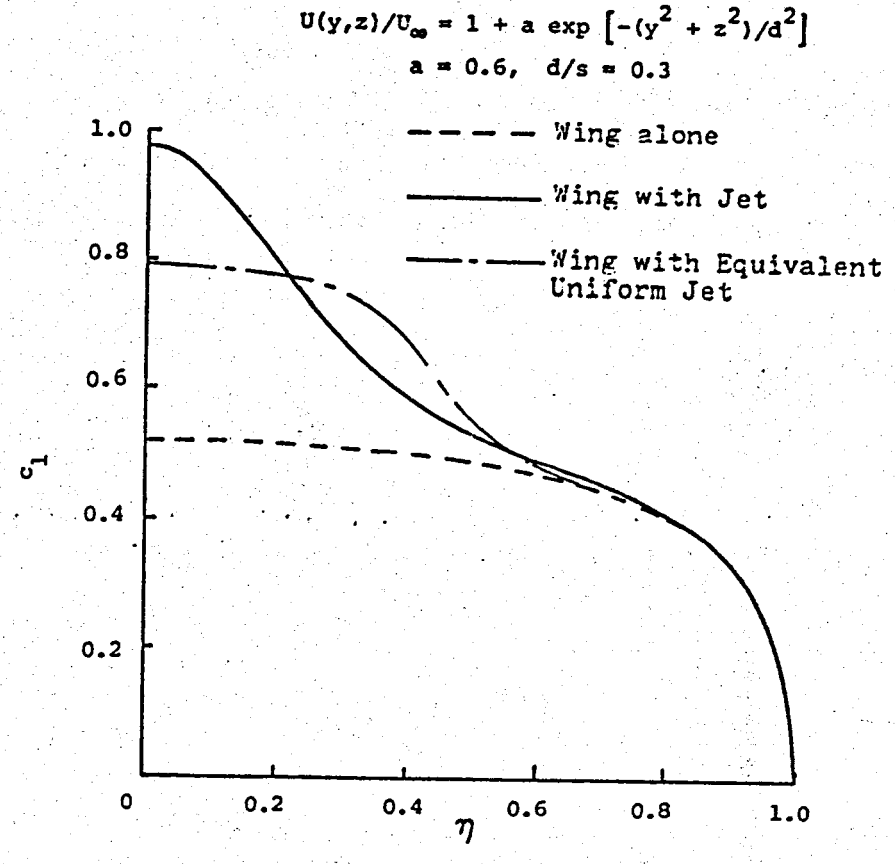

Fig. 3.5 Spanwise lift distribution on a rectangular wing of AR = 6.0 at α = 0.1 radian.

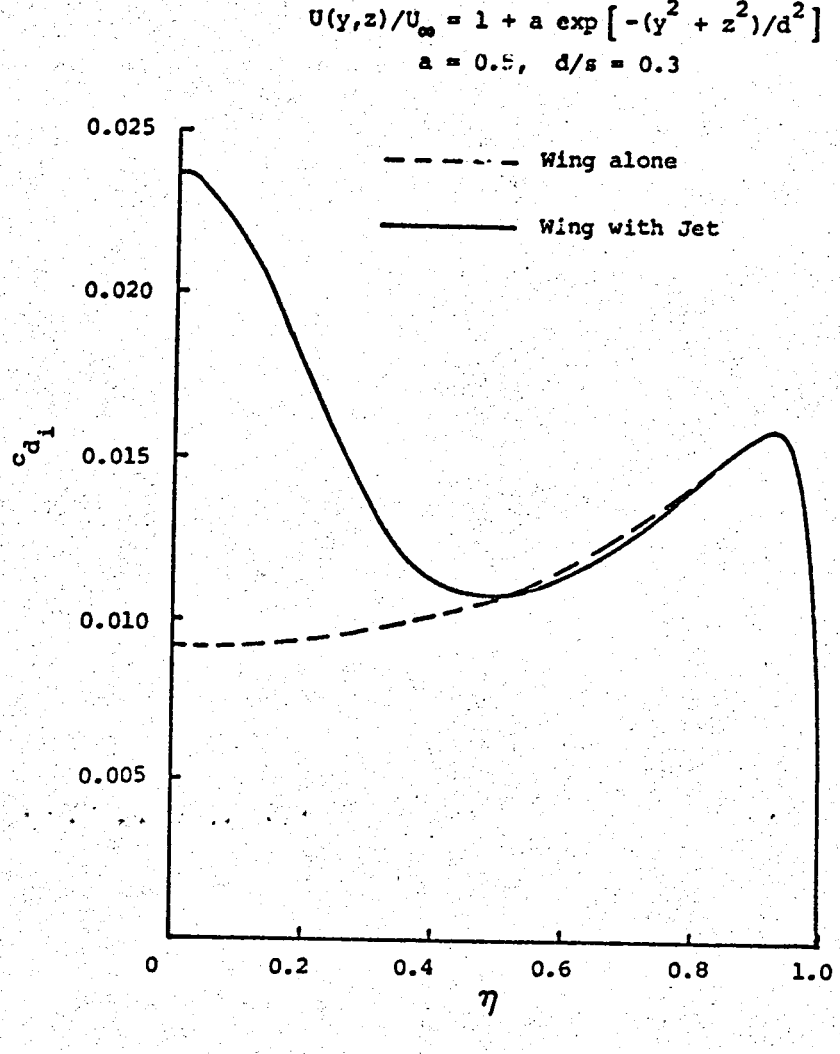

Fig. 3.6 Spanwise induced drag distribution on a rectangular wing of AR = 6.0 at α = 0.1 radian.

$$U(y,z)/U_\infty = 1 + a_1 \exp\left[-(y^2 + z^2)/d_1^2\right] - a_2 \exp\left[-(y^2 + z^2)/d_2^2\right]$$

$a_1 = 0.6$, $a_2 = 0.75$, $d_1/s = 0.3$, $d_2/s = 0.05$

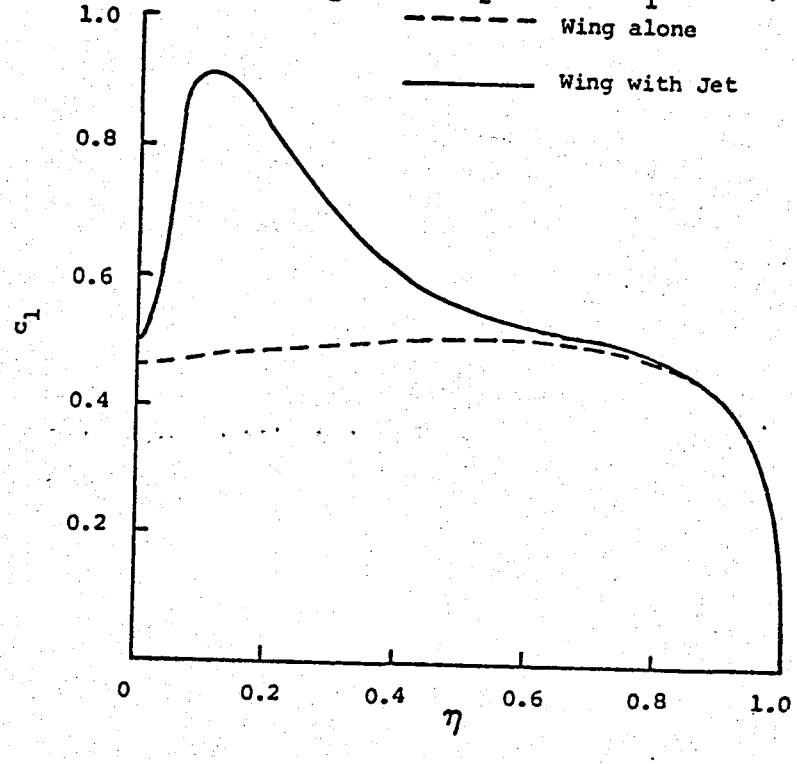

Fig. 3.7 Spanwise lift distribution on a tapered wing of AR = 6.67, $\lambda = 0.5$ at $\alpha = 0.1$ radian.

effect of the nonuniformity on the lift distribution. Figure 3.8 illustrates the spanwise induced drag distribution on the wing.

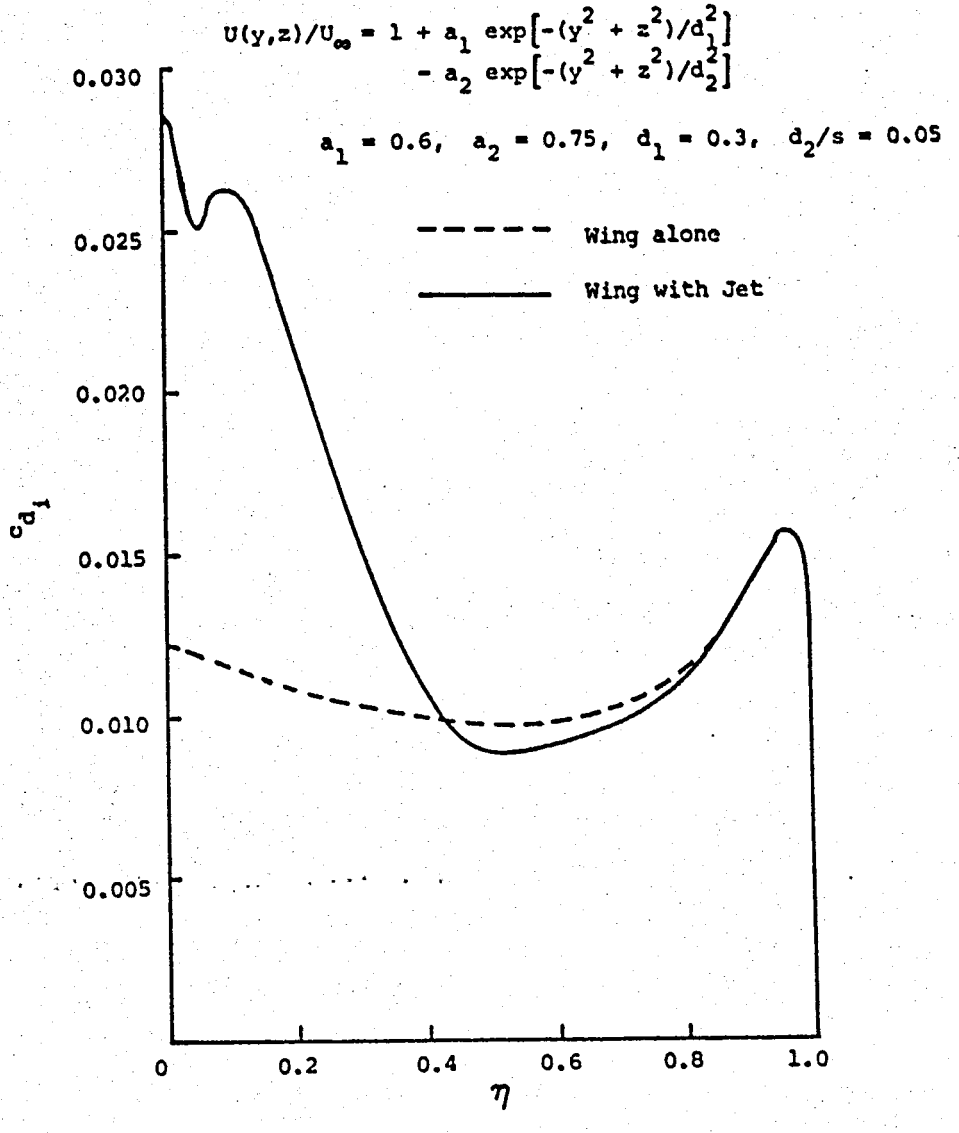

Fig. 3.8 Spanwise induced drag distribution on a tapered wing of AR = 6.67, $\lambda = 0.5$ at $\alpha = 0.1$ radian.

This Page Intentionally Left Blank

Chapter 4

AN ASYMPTOTIC THEORY FOR THE INTERFERENCE OF SWEPT WINGS AND MULTIPLE SLIPSTREAMS

The asymptotic method was employed by Van Dyke [28] for the analysis of large aspect ratio wings in uniform flow. This method was subsequently applied to wings with jet flaps by Kerney [33] and Takuda [34]. Ting, et al. [15] applied this method to study the interference of unswept wings and multiple propeller slipstreams. As noted earlier, the asymptotic method is simple and provides physical insight into the problem. The present chapter deals with an extension of Ting's method to swept wings, i.e., the application of the asymptotic method to the problem of interference of large aspect ratio swept wings and multiple propeller slipstreams.

4.1 Mathematical Formulation

Consider a large aspect ratio swept wing in a uniform flow (Fig. 4.1). Propellers placed ahead of the wing produce slipstreams which flow past the wing. It is assumed that the wing geometry and the velocity distribution in the slipstream are known. The problem is to determine the lift distribution on the wing as influenced by the slipstream.

In the present analysis, the flow is considered to be steady, incompressible and inviscid. This amounts to a considerable simplification; however, the resulting problem is nonlinear due to the

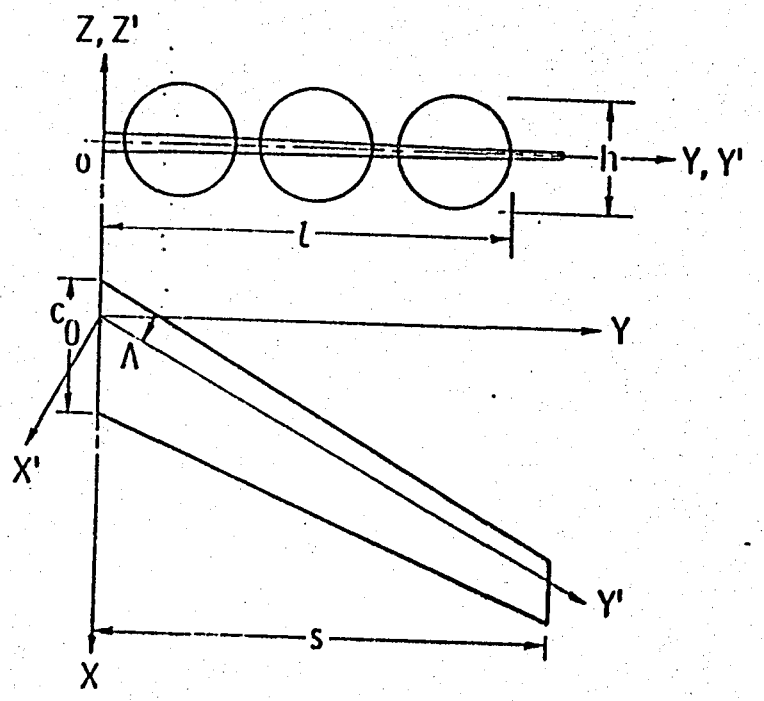

Fig. 4.1 Schematic of the swept wing - slipstream interference problem.

nonuniform flow in the slipstream, and the governing equations are the Euler equations.

In the analysis that follows, two right-handed Cartesian coordinate systems are used. The (x,y,z) system has the x-axis in the direction of the free stream and the z-axis in the lift direction. The (x',y',z') system is obtained by rotation of the first system through the quarter chord sweep angle Λ about the z-axis. It should be noted that the z'-axis is identical to the the z-axis and that the y'-axis lies along the quarter-chord line of the wing planform.

In the absence of the wing, it is assumed that the undisturbed velocity field can be written as follows:

$$\vec{V}(x/c_0, y/s, z/c_0) = \vec{i}\, U_\infty \qquad \text{(ahead of the propellers)} \qquad (4.1a)$$

$$= \vec{i}\, U(y/s, z/c_0) \qquad \text{(behind the propellers)} \qquad (4.1b)$$

$$= \vec{i}\, U_\infty \qquad \text{(for large } |z|\text{)} \qquad (4.1c)$$

where $\vec{i}$ is the unit vector in the x-direction. This amounts to assuming that there is a jump in the axial velocity across the propellers and that there is no swirl in the propeller stream. The velocity field around a propeller is quite complex. There is inflow ahead of the propeller. There is a pressure jump and not a velocity jump across the propeller. The velocity field in the slipstream is periodic rather than steady because of the finite number of blades, and has the swirl component in addition to an increased axial velocity. In spite of this, the drastic idealization implied in Eq. (4.1) for the velocity field around the propellers is quite common, and springs from the fact that detailed treatment of the swirl and periodicity in the stream makes the

problem extremely complex. Attempts have been made by several workers to take into account the effects of the swirl in a simplified manner by assuming that the swirl only introduces a change in the spanwise distribution of the sectional angle of attack. In the absence of any superior approach, this simple method is adopted in the present study.

The analysis starts by making the assumption that for large aspect ratio wings with multiple tractor propellers, the height (h) of the slipstream behind the propellers is of the order of the mid-chord c_0, whereas the spanwise spread (2ℓ) of the combined propeller slipstreams is of the order of the wing span b=2s. Thus there are two length scales c_0 and b in the problem; hence, different stretching transformations are possible. Following the classical analysis for large aspect ratio wings, the outer region is introduced with the corresponding stretched variables $\tilde{x},\tilde{y},\tilde{z}$ defined as follows:

$$\tilde{x} = x/s, \quad \tilde{y} = y/s \quad \text{and} \quad \tilde{z} = z/s \tag{4.2}$$

With $\tilde{x},\tilde{y},\tilde{z}$ fixed and AR$\to\infty$ (or $\varepsilon\to 0$, where $\varepsilon=c_0/s$), the wing shrinks to a line, in which all the singularities that may be used to represent it are concentrated. The undisturbed velocity becomes

$$\vec{V} = \vec{i}\, U_\infty \qquad \text{(ahead of the wing)} \tag{4.3a}$$

$$= \vec{i}\, U_\infty \qquad \text{(behind the wing except on the cut z=0)} \tag{4.3b}$$

The momentum gained by the stream in passing through the propeller is now contained in this thin sheet which acts very much like a jet flap. The spanwise distribution of the momentum in this sheet is given by

$$J(\tilde{y}) = \rho c_0 \int_{-\infty}^{\infty} U(U - U_\infty)d\tilde{z} \tag{4.4}$$

All the details of the flow past the wing section are lost in this outer limiting process. To recover these details, the inner region is introduced with the inner variables $\hat{x}$, $\hat{y}$, and $\hat{z}$ defined by the following transformation:

$$\hat{x} = x'/c_0, \quad \hat{y} = y'/s \quad \text{and} \quad \hat{z} = z'/c_0 \tag{4.5}$$

The following relations exist between the variables $(\hat{x},\hat{y},\hat{z})$ and (x',y',z'):

$$x' = \hat{x}\cos\Lambda + \hat{y}\sin\Lambda, \quad y' = \hat{y}\cos\Lambda - \hat{x}\sin\Lambda \quad \text{and} \quad z' = \hat{z} \tag{4.6}$$

Now, the undisturbed velocity behind the propellers can be expressed as

$$\begin{aligned}
\vec{V}(x/c_0,y/s,z/c_0) &= \vec{i}\, U(y/s,z/c_0) \\
&= \vec{i}\, U[(y'\cos\Lambda - x'\sin\Lambda)/s, z'/c_0] \\
&= \vec{i}\, U[(\hat{y}\cos\Lambda - \epsilon\hat{x}\sin\Lambda), \hat{z}] \\
&= \vec{i}\, [U(\hat{y}\cos\Lambda,\hat{z}) - \epsilon\hat{x}\tan\Lambda \frac{\partial U}{\partial y}(\hat{y}\cos\Lambda,\hat{z}) + \ldots] \\
&= \vec{i}\, U(\hat{y}\cos\Lambda,\hat{z}) \quad \text{for } \epsilon << 1
\end{aligned} \tag{4.7}$$

The undisturbed stream for the inner region, therefore, is given by (in the transformed coordinate system)

$$\vec{V} = [U(\hat{y}\cos\Lambda,\hat{z})\cos\Lambda,\ U(\hat{y}\cos\Lambda,\hat{z})\sin\Lambda,\ 0] \tag{4.8}$$

The analysis of the flow in the propeller stream behind the wing requires the introduction of another region (called the third region) with the corresponding variables $\bar{x},\bar{y}$ and $\bar{z}$ defined as follows:

$$\bar{x} = x/s, \quad \bar{y} = y/s \quad \text{and} \quad \bar{z} = z/c_0 \tag{4.9}$$

In this region, the undisturbed velocity is given by

$$\vec{V} = \vec{i}\, U(y/s, z/c_0) = \vec{i}\, U(\bar{y},\bar{z}) \tag{4.10}$$

The three flow regions are shown schematically in Fig. 4.2. Equations (4.3),(4.8) and (4.10) represent the undisturbed velocity field for the three regions considered. The effect of the presence of the wing is to introduce disturbances in these flowfields. The disturbances in velocity and pressure depend on the small parameter $\varepsilon=c_0/s$ which, in turn, is related to the reciprocal of the wing aspect ratio. In the following sections, these disturbances are introduced in the flowfields of the three regions, and the governing equations are derived. The solution obtained in each region is matched with the others as described in Sec. 4.4, and a solution for the entire problem is obtained.

4.2 The Inner Region

The disturbances in velocity components and pressure for the inner region are expanded in power series of ε as follows:

$$\hat{u}(\hat{x},\hat{y},\hat{z};\varepsilon) = \hat{u}^{(0)}(\hat{x},\hat{y},\hat{z}) + \varepsilon\hat{u}^{(1)}(\hat{x},\hat{y},\hat{z}) + \ldots \tag{4.11a}$$

$$\hat{v}(\hat{x},\hat{y},\hat{z};\varepsilon) = \hat{v}^{(0)}(\hat{x},\hat{y},\hat{z}) + \varepsilon\hat{v}^{(1)}(\hat{x},\hat{y},\hat{z}) + \ldots \tag{4.11b}$$

$$\hat{w}(\hat{x},\hat{y},\hat{z};\varepsilon) = \hat{w}^{(0)}(\hat{x},\hat{y},\hat{z}) + \varepsilon\hat{w}^{(1)}(\hat{x},\hat{y},\hat{z}) + \ldots \tag{4.11c}$$

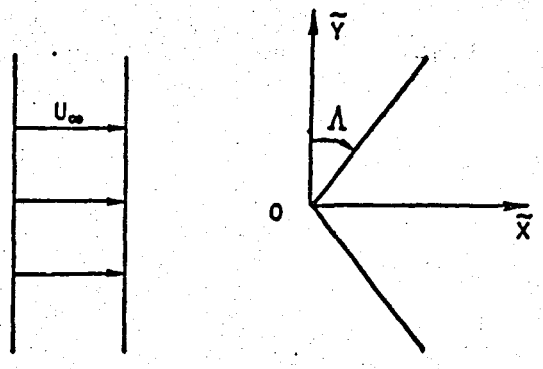

a) The Outer Region

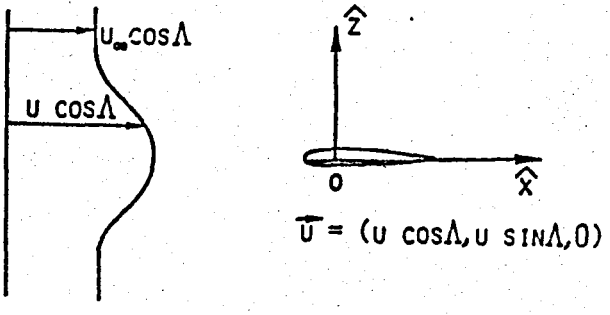

b) The Inner Region

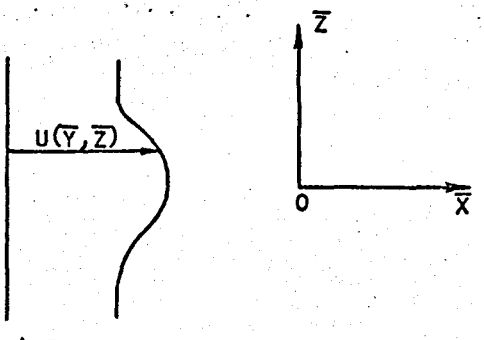

c) The Third Region

Fig. 4.2 The three flow regions.

$$\hat{p}(\hat{x},\hat{y},\hat{z};\epsilon) = \hat{p}^{(0)}(\hat{x},\hat{y},\hat{z}) + \epsilon\hat{p}^{(1)}(\hat{x},\hat{y},\hat{z}) + \ldots \tag{4.11d}$$

The undisturbed velocity components given by Eq. (4.8) and the disturbance quantities given by Eq. (4.11) are substituted in the continuity and the momentum equations. Upon equating the coefficients of like powers of ϵ on either side of the equations, the following leading equations are obtained:

$$\hat{u}^{(0)}_{\hat{x}} + \hat{w}^{(0)}_{\hat{z}} = 0 \tag{4.12}$$

$$(U\cos\Lambda + \hat{u}^{(0)})\hat{u}^{(0)}_{\hat{x}} + \hat{w}^{(0)}(U\cos\Lambda + \hat{u}^{(0)})_{\hat{z}} = -\hat{p}^{(0)}_{\hat{x}}/\rho \tag{4.13a}$$

$$(U\cos\Lambda + \hat{u}^{(0)})\hat{v}^{(0)}_{\hat{x}} + \hat{w}^{(0)}(U\sin\Lambda + \hat{v}^{(0)})_{\hat{z}} = 0 \tag{4.13b}$$

$$(U\cos\Lambda + \hat{u}^{(0)})\hat{w}^{(0)}_{\hat{x}} + \hat{w}^{(0)}\hat{w}^{(0)}_{\hat{z}} = -\hat{p}^{(0)}_{\hat{z}}/\rho \tag{4.13c}$$

If a stream function $\hat{\phi}^{(0)}(\hat{x},\hat{y},\hat{z})$ is defined such that

$$\hat{\phi}^{(0)}_{\hat{z}} = U\cos\Lambda + \hat{u}^{(0)} \tag{4.14a}$$

$$\hat{\phi}^{(0)}_{\hat{x}} = -\hat{w}^{(0)} \tag{4.14b}$$

then Eq. (4.12) is automatically satisfied. Now, it should be noted that Eqs. (4.13a) and (4.13c) do not involve the $\hat{v}$-component of the velocity, and that by eliminating the pressure, they can be reduced to the two-dimensional vorticity transport equation

$$(U\cos\Lambda + \hat{u}^{(0)})\omega_{\hat{x}} + \hat{w}^{(0)}\omega_{\hat{z}} = 0 \tag{4.15}$$

where

$$\omega = \hat{w}^{(0)}_{\hat{x}} - (U\cos\Lambda + \hat{u}^{(0)})_{\hat{z}} = -(\hat{\phi}^{(0)}_{\hat{x}\hat{x}} + \hat{\phi}^{(0)}_{\hat{z}\hat{z}}) \tag{4.16}$$

A combination of Eqs. (4.14a), (4.14b) and (4.15) results in

$$\hat{\phi}^{(0)}_{\hat{z}}\omega_{\hat{x}} - \hat{\phi}^{(0)}_{\hat{x}}\omega_{\hat{z}} = 0 \tag{4.17}$$

This implies that ω is a function of $\hat{\phi}^{(0)}$ only, or equivalently ω is constant along $\hat{\phi}^{(0)}$=constant (i.e., along the projection of the streamlines on the $\hat{y}$=constant plane). Thus, the problem reduces to solving the Poisson equation

$$\omega(\hat{\phi}^{(0)}) = -(\phi^{(0)}_{\hat{x}\hat{x}} + \hat{\phi}^{(0)}_{\hat{z}\hat{z}}) \tag{4.18}$$

This equation applies to the flowfield behind the propellers. In the plane of the propellers, the disturbances due to the wing section may be neglected. Consequently, the boundary condition at the propeller plane would be

$$\hat{\phi}^{(0)} = \int_0^{\hat{z}} U\, d\hat{z} \tag{4.19}$$

The other boundary conditions are (1) far away from the airfoil $\hat{u}^{(0)}$ and $\hat{w}^{(0)}$ tend to zero, (2) on the airfoil the normal velocity component is zero, and (3) at the trailing edge of the airfoil the pressure is continuous (which is equivalent to the Kutta condition). Note that in

this problem, $\hat{y}$ appears only as a parameter.

The solution of Eq. (4.18), or the equivalent Eq. (4.12), (4.13a) and (4.13c), with the above boundary conditions can be obtained by a suitable numerical technique. The results would yield the values of the velocity components $\hat{u}^{(0)}$ and $\hat{w}^{(0)}$ everywhere in the field including the airfoil surface.

The $\hat{y}$-momentum equation, Eq. (4.13b), may be rewritten as follows:

$$[(U\cos\Lambda + \hat{u}^{(0)})\frac{\partial}{\partial\hat{x}} + \hat{w}^{(0)}\frac{\partial}{\partial\hat{z}}](U\sin\Lambda + \hat{v}^{(0)}) = 0$$

or

$$\frac{\partial}{\partial s}(U\sin\Lambda + \hat{v}^{(0)}) = 0 \qquad (4.20)$$

where $\frac{\partial}{\partial s} = (U\cos\Lambda + \hat{u}^{(0)})\frac{\partial}{\partial\hat{x}} + \hat{w}^{(0)}\frac{\partial}{\partial\hat{z}}$. Note that $\frac{\partial}{\partial s}$ is the derivative along the projection of the streamline in the $\hat{x}$-$\hat{z}$ plane. Equation (4.20) implies that $(U\sin\Lambda + \hat{v}^{(0)})$ remains constant along the streamlines projected on the $\hat{x}$-$\hat{z}$ planes. Since the airfoil is one such streamline it is concluded that $(U\sin\Lambda + \hat{v}^{(0)})$ is a constant on the airfoil. Let U^* be the velocity far ahead of the airfoil on the zero streamline. Then, it is evident that $U^*\sin\Lambda = (U\sin\Lambda + \hat{v}^{(0)})$. Note that, even though $(U\sin\Lambda + \hat{v}^{(0)})$ is a constant on the airfoil, both $U\sin\Lambda$ and $\hat{v}^{(0)}$ being functions of $\hat{z}$, vary along the airfoil surface.

The pressure coefficient c_p on the airfoil defined by

$$c_p = (p-p_\infty)/(1/2)\rho U_\infty^2 \qquad (4.21)$$

can be reduced to

$$c_p(\hat{x},\hat{z}) = [U^{*2}\cos^2\Lambda - (U\cos\Lambda + \hat{u}^{(0)})^2 - (\hat{w}^{(0)})^2]/U_\infty^2 \qquad (4.22)$$

Hence the difference Δc_p is given by

$$\Delta c_p(\hat{x}) = c_p(\hat{x},\hat{z}_\ell) - c_p(\hat{x},\hat{z}_u)$$
$$= -\{(U\cos\Lambda + \hat{u}^{(0)})^2 + (\hat{w}^{(0)})^2\}/U_\infty^2 \qquad (4.23)$$

where $\{\ \}$ represents the difference between the lower and the upper surfaces of the airfoil. The sectional lift coefficient c_ℓ is obtained by integration of $\Delta c_p(\hat{x})$ along the chord. Thus, it is seen that the lift obtained by the solution of Eq. (4.13) is not affected by the spanwise component of the velocity. In summary, the governing equations for the inner solution are the continuity and momentum Eqs. (4.12) and (4.13), with the appropriate boundary conditions. The solution of these would yield the lift of the airfoil which is independent of the spanwise velocity component. This lift is a function of the sectional angle of attack, and may be written as follows:

$$\ell(\alpha,\hat{y}) = (1/2)\rho U_\infty^2 c(\hat{y}) c_\ell(\alpha,\hat{y}) \qquad (4.24)$$

Notice that in this relation $\hat{y}$ appears only as a parameter.

4.3 The Third Region

In the analysis of the third region, i.e., in the propeller stream far behind the wing, the stretched coordinates $\bar{x},\bar{y}$ and $\bar{z}$ defined by Eq. (4.9), and the undisturbed velocity defined by Eq. (4.10) are used. The perturbation velocity components and the pressure are expressed in power series of ε as follows:

$$\bar{u}(\bar{x},\bar{y},\bar{z};\varepsilon) = \bar{u}^{(0)}(\bar{x},\bar{y},\bar{z}) + \varepsilon\bar{u}^{(1)}(\bar{x},\bar{y},\bar{z})$$

$$+ \varepsilon^2 \bar{u}^{(2)}(\bar{x},\bar{y},\bar{z}) + \ldots \qquad (4.25a)$$

$$\bar{v}(\bar{x},\bar{y},\bar{z};\varepsilon) = \varepsilon \bar{v}^{(1)}(\bar{x},\bar{y},\bar{z}) + \varepsilon^2 \bar{v}^{(2)}(\bar{x},\bar{y},\bar{z}) + \ldots \qquad (4.25b)$$

$$\bar{w}(\bar{x},\bar{y},\bar{z};\varepsilon) = \varepsilon \bar{w}^{(1)}(\bar{x},\bar{y},\bar{z}) + \varepsilon^2 \bar{w}^{(2)}(\bar{x},\bar{y},\bar{z}) + \ldots \qquad (4.25c)$$

$$\bar{p}(\bar{x},\bar{y},\bar{z};\varepsilon) = \varepsilon \bar{p}^{(1)}(\bar{x},\bar{y},\bar{z}) + \varepsilon^2 \bar{p}^{(2)}(\bar{x},\bar{y},\bar{z}) + \ldots \qquad (4.25d)$$

These perturbation components and the undisturbed velocity given by Eq. (4.10) are substituted in the continuity and momentum equations. The subsequent analysis would be identical to the analysis performed in [15] while studying the third region behind unswept wings. Therefore these details are not given here; but only the major conclusions from this analysis are listed below:

(1) To the first order, there is no pressure discontinuity or change in streamline inclination across the jet sheet.

(2) The momentum integral $J(\bar{y})$ remains constant with respect to $\bar{x}$.

(3) To the second order, there is a pressure difference across the jet sheet given by

$$\Delta\tilde{p}^{(2)} = \tilde{p}^{(2)}(\tilde{x},\tilde{y},0+) - \tilde{p}^{(2)}(\tilde{x},\tilde{y},0-) = -\varepsilon \tilde{\theta}^{(1)}_{\tilde{x}}(\tilde{x},\tilde{y},0) J(\tilde{y}) \qquad (4.26)$$

where

$$\tilde{\theta}^{(1)} = \tilde{w}^{(1)}/U_\infty$$

Equation (4.26) is the familiar result of the thin jet approximation that states the pressure difference across the sheet is equal to the product of the momentum in the jet sheet and its curvature. These

results will be used in the analysis of the outer region that follows.

4.4 The Outer Region

The undisturbed velocity in the outer region is uniform (Eqs. (4.3a) and (4.3b)); hence, the flowfield away from the wing and the propeller streams is irrotational. Therefore the disturbance velocity field can be described by a velocity potential $\tilde{\Phi}(\tilde{x},\tilde{y},\tilde{z};\varepsilon)$ which satisfies the Laplace equation

$$\left(\frac{\partial^2}{\partial\tilde{x}^2} + \frac{\partial^2}{\partial\tilde{y}^2} + \frac{\partial^2}{\partial\tilde{z}^2}\right)\tilde{\Phi} = 0 \tag{4.27}$$

Bernoulli's equation provides an expression for the pressure disturbances as

$$\tilde{p} = (1/2)\rho U_\infty^2\left[1 - \left|\vec{i} + \nabla\tilde{\Phi}/U_\infty\right|^2\right] \tag{4.28}$$

Equations (4.1) and (4.2) are the governing equations in the outer region. As the first step towards the solution, Φ is expanded in a power series of ε as

$$\tilde{\Phi}(\tilde{x},\tilde{y},\tilde{z};\varepsilon) = \varepsilon\tilde{\Phi}^{(1)}(\tilde{x},\tilde{y},\tilde{z}) + \varepsilon^2\tilde{\Phi}^{(2)}(\tilde{x},\tilde{y},\tilde{z}) + \ldots \tag{4.29}$$

where both $\tilde{\Phi}^{(1)}$ and $\tilde{\Phi}^{(2)}$ in turn satisfy the Laplace Eq. (4.27). Next the velocity and pressure disturbances are also expanded in power series of ε as follows:

$$\tilde{u}(\tilde{x},\tilde{y},\tilde{z};\varepsilon) = \varepsilon\tilde{u}^{(1)}(\tilde{x},\tilde{y},\tilde{z}) + \varepsilon^2\tilde{u}^{(2)}(\tilde{x},\tilde{y},\tilde{z}) + \ldots \tag{4.30a}$$

$$\tilde{v}(\tilde{x},\tilde{y},\tilde{z};\varepsilon) = \varepsilon\tilde{v}^{(1)}(\tilde{x},\tilde{y},\tilde{z}) + \varepsilon^2\tilde{v}^{(2)}(\tilde{x},\tilde{y},\tilde{z}) + \ldots \tag{4.30b}$$

$$\tilde{w}(\tilde{x},\tilde{y},\tilde{z};\varepsilon) = \varepsilon\tilde{w}^{(1)}(\tilde{x},\tilde{y},\tilde{z}) + \varepsilon^2\tilde{w}^{(2)}(\tilde{x},\tilde{y},\tilde{z}) + \ldots \qquad (4.30c)$$

$$\tilde{p}(\tilde{x},\tilde{y},\tilde{z};\varepsilon) = \varepsilon\tilde{p}^{(1)}(\tilde{x},\tilde{y},\tilde{z}) + \varepsilon^2\tilde{p}^{(2)}(\tilde{x},\tilde{y},\tilde{z} + \ldots \qquad (4.30d)$$

Thus,

$$\tilde{u}^{(1)} = \tilde{\Phi}^{(1)}_{\tilde{x}}(\tilde{x},\tilde{y},\tilde{z})/s \qquad (4.31a)$$

$$\tilde{v}^{(1)} = \tilde{\Phi}^{(1)}_{\tilde{y}}(\tilde{x},\tilde{y},\tilde{z})/s \qquad (4.31b)$$

$$\tilde{w}^{(1)} = \tilde{\Phi}^{(1)}_{\tilde{z}}(\tilde{x},\tilde{y},\tilde{z})/s \qquad (4.31c)$$

$$\tilde{p}^{(1)} = \rho U_\infty \tilde{\Phi}^{(1)}_{\tilde{x}}(\tilde{x},\tilde{y},\tilde{z})/s \qquad (4.31d)$$

The unknown $\tilde{\Phi}^{(1)}$ is a solution of the Laplace equation. It is obtained by distributing the singularities along the line $\tilde{x}-m|\tilde{y}|=0$, and on the plane $\tilde{z}=0$, $\tilde{x}-m|\tilde{y}|>0$, and by matching with the solutions of the inner and the third regions respectively. Note that m is the tangent of the wing quarter chord sweep-back angle.

By an analysis of the inner region it was shown that the wing section at a spanwise station $\tilde{y}$ produces a lift force $\ell(\alpha,\tilde{y})$ (Eq. 4.24). This implies that there is a vortex distribution along the line $\tilde{x}-m|\tilde{y}|=0$. The strength $\Gamma(\tilde{y})$ is related to the lift $\ell(\alpha,\tilde{y})$ as follows:

$$\Gamma(\tilde{y}) = \ell(\alpha,\tilde{y})/\rho U_\infty$$

$$= (1/2)U_\infty c(\tilde{y}) c_\ell(\alpha,\tilde{y}) \qquad (4.32)$$

The spanwise variation of Γ requires the presence of a trailing vortex sheet extending downstream from the lifting line. This is the well known vortex system of lifting-line theory.

By a matching with the solution of the third region, it was shown that, to a first approximation, there is no discontinuity in either the pressure or the streamline inclination across the jet sheet behind the wing. Therefore, the first order outer solution $\tilde{\Phi}^{(1)}$ is not affected by the propeller stream behind the lifting line. Based on this first order analysis, the flow in the outer region is described by the potential due to $\Gamma(\tilde{y})$ and the associated trailing vortex system, and is given by

$$\tilde{\Phi}^{(1)} = \frac{1}{4\pi}\int_{-1}^{1} \frac{\tilde{z}\Gamma(\eta)}{(\tilde{y}-\eta)^2 + \tilde{z}^2}\left\{1 + \frac{\tilde{x}-m|\eta|}{R}\right\} d\eta \qquad (4.33)$$

where $R^2 = [(\tilde{x}-m|\eta|)^2 + (\tilde{y}-\eta)^2 + \tilde{z}^2]$. Upon approaching the lifting line (i.e., for small $\tilde{x}-m|\tilde{y}|$ and $\tilde{z}$), the inner limit of $\tilde{\Phi}^{(1)}$ is obtained. This yields the downwash $\theta(\tilde{x}-m|\tilde{y}|\to 0,\tilde{y},0)$. By matching with the inner solution, the effective angle of attack at each spanwise station is obtained as

$$\alpha(\tilde{y}) = \alpha_g(\tilde{y}) - \varepsilon\tilde{\theta}^{(1)} = \alpha_g(\tilde{y}) - \tilde{\theta} \qquad (4.34)$$

The circulation $\Gamma(\tilde{y})$, given by Eq. (4.32), now becomes

$$\Gamma(\tilde{y}) = (1/2)U_\infty c(\tilde{y})c_\ell(\alpha_g - \tilde{\theta};\ \tilde{y}) \qquad (4.35)$$

Equations (4.34) and (4.35) are the required governing equations for the first order analysis. Note that in this analysis, the effect of the nonuniform flow in the slipstream enters only in the sectional analysis.

The first order analysis discussed so far is valid for $\varepsilon \to 0$, or $AR \to \infty$. It was shown in the analysis of the third region that terms proportional to $J(\tilde{y})$ appear in the second order analysis; hence it is necessary that $J(\tilde{y})$ be of the order of 1.0 for the first-order theory to be valid. It is well known that the first order theory for large aspect ratio wings in uniform flow gives satifactory results for wings of aspect ratio as low as 1.0 [33]. Hence, only the contribution of the momentum in the propeller stream will be considered in an extension of the present analysis.

At the outset it is noted that $\tilde{\Phi}^{(1)}$ is an odd function in $\tilde{z}$. It was shown by an analysis of the third region that $\tilde{p}^{(1)}(\tilde{x},\tilde{y},\tilde{z})$ is continuous across $\tilde{z}=0$. Hence it is concluded that

$$\tilde{p}^{(1)}(\tilde{x},\tilde{y},\tilde{z}=0) = 0 \tag{4.36}$$

In view of Eq. (4.31a) and (4.31d), it may also be stated that behind the wing

$$\tilde{u}^{(1)}(\tilde{x},\tilde{y},\tilde{z}=0) = 0 \tag{4.37}$$

However, because of the vorticity $d\Gamma(\tilde{y})/d\tilde{y}$ on the plane $\tilde{z}=0$ behind the wing, $\tilde{v}^{(1)}$ is discontinuous across the jet sheet and is given by

$$\tilde{v}^{(1)}(\tilde{x},\tilde{y},\tilde{z}=0+) = d\Gamma(\tilde{y})/d\tilde{y} = -\tilde{v}^{(1)}(\tilde{x},\tilde{y},\tilde{z}=0-) \tag{4.38}$$

Nevertheless, $[\tilde{v}^{(1)}]^2$ is continuous across the jet sheet. Furthermore, since $\tilde{\theta}^{(1)}$ is continuous, $\tilde{w}^{(1)}$ is also continuous across the jet sheet.

Next, upon considering the $O(\varepsilon^2)$ terms in the Bernoulli equation the following equation is obtained:

$$\tilde{p}^{(2)}/\rho = - U_\infty \tilde{u}^{(2)} - [(\tilde{v}^{(1)})^2 + (\tilde{w}^{(1)})^2]/2 \qquad (4.39)$$

Since $[\tilde{v}^{(1)}]^2$ and $\tilde{w}^{(1)}$ are continuous, the pressure difference across the sheet is given simply by

$$\Delta\tilde{p}^{(2)} = \tilde{p}^{(2)}(\tilde{x},\tilde{y},\tilde{z}=0+) - \tilde{p}^{(2)}(\tilde{x},\tilde{y},\tilde{z}=0-)$$

$$= -\rho U_\infty [\tilde{u}^{(2)}(\tilde{x},\tilde{y},\tilde{z}=0+) - \tilde{u}^{(2)}(\tilde{x},\tilde{y},\tilde{z}=0-)] \qquad (4.40)$$

This discontinuity in $\tilde{u}^{(2)}$ is equivalent to a vorticity distribution $\gamma(\tilde{x},\tilde{y})$ on the jet sheet and, in view of Eq. (4.26), $\gamma(\tilde{x},\tilde{y})$ can be expressed as

$$\gamma(\tilde{x},\tilde{y}) = - \varepsilon \underset{\tilde{x}}{\tilde{\theta}}^{(1)}(\tilde{x},\tilde{y},0) J(\tilde{y})/\rho U_\infty s = - \underset{\tilde{x}}{\tilde{\theta}}(\tilde{x},\tilde{y},0) J(\tilde{y})/\rho U_\infty s \qquad (4.41)$$

At the lifting line, $\tilde{\theta}$ is not zero (i.e., the jet sheet has a non-zero inclination at the lifting line). This would require a vertical force of magnitude $J(\tilde{y})\varepsilon\tilde{\theta}^{(1)}$ at the lifting line. To account for this force, a circulation distribution $\Gamma_J(\tilde{y})$ is introduced along the lifting line. The magnitude of this circulation is given by

$$\Gamma_J(\tilde{y}) = - J(\tilde{y})\varepsilon\tilde{\theta}^{(1)}/\rho U_\infty = - J(\tilde{y})\tilde{\theta}/\rho U_\infty \qquad (4.42)$$

Thus, in this limited second order analysis, referred to as the systematic analysis in [15], the vortex system consists of the circulation $\Gamma(\tilde{y})$ along the lifting line, the circulation $\Gamma_J(\tilde{y})$ which accounts for the change in the inclination of the jet sheet on passing over the wing, and a distribution $\gamma(\tilde{x},\tilde{y})$ behind the wing, which accounts for the curvature of the jet sheet. This system of vortices produces a downwash distribution $\theta(\tilde{x},\tilde{y})$ which is obtained from the following

velocity potential:

$$\Phi(\tilde{x},\tilde{y},\tilde{z}) = \frac{1}{4\pi}\int_{-1}^{1} \frac{\tilde{z}\Gamma(\eta)}{\tilde{z}^2 + (\tilde{y}-\eta)^2}\left\{1 + \frac{\tilde{x}-m|\eta|}{R}\right\} d\eta$$

$$+ \frac{1}{4\pi}\int_{-\ell}^{\ell} \frac{\tilde{z}\Gamma_J(\eta)}{\tilde{z}^2 + (\tilde{y}-\eta)^2}\left\{1 + \frac{\tilde{x}-m|\eta|}{R}\right\} d\eta$$

$$+ \frac{1}{4\pi}\int_{-\ell}^{\ell}\int_{m|\eta|}^{\infty} \frac{\tilde{z}\gamma(\xi,\eta)}{\tilde{z}^2 + (\tilde{y}-\eta)^2}\left\{1 + \frac{(\tilde{x}-\xi)}{\sqrt{[(\tilde{x}-\xi)^2 + (\tilde{y}-\eta)^2 + \tilde{z}^2]}}\right\} d\xi\, d\eta \quad (4.43)$$

The downwash is related to the unknown quantities by the following relations:

$$\Gamma(\tilde{y}) = (1/2)U_\infty c(\tilde{y}) c_{\ell_\alpha}[\alpha_g(\tilde{y}) - \tilde{\theta}(\tilde{x},\tilde{y})], \qquad \tilde{x} \to m|\tilde{y}| \quad (4.44)$$

$$\Gamma_J(\tilde{y}) = -J(\tilde{y})\tilde{\theta}(\tilde{x},\tilde{y})/\rho U_\infty, \qquad \tilde{x} \to m|\tilde{y}| \quad (4.45)$$

$$\gamma(\tilde{x},\tilde{y}) = -J(\tilde{y})\tilde{\theta}_{\tilde{x}}(\tilde{x},\tilde{y})/\rho U_\infty s \quad (4.46)$$

These are the governing equations for the unknowns $\Gamma(\tilde{y})$, $\Gamma_J(\tilde{y})$ and $\gamma(\tilde{x},\tilde{y})$.

4.5 Method of Solution

The governing equations for the unknowns $\Gamma(y)$, $\Gamma_J(y)$ and $\gamma(\tilde{x},\tilde{y})$ are the Eqs. (4.44) - (4.46) together with the Eq. (4.43) for the downwash angle $\tilde{\theta}$ required in the solution. The downwash angle computed by Eq. (4.43) on the lifting line at the wing centerline is infinite because of the discontinuity in the slope of the lifting line at the wing root. This is a familiar problem in the swept wing analysis.

Rigorous studies of swept wings in uniform flow by Cheng, et al. [36,37] have shown that the induced velocity approaches infinity like the logarithm of the distance from the centerline. This behavior does not allow computation of the spanload at the wing centerline of symmetrically swept wings. Thurber [38] studied swept wings with curved centerlines having zero sweep at the wing centerline and zero tip chord (crescent wings) in uniform flow. This planform has limited application in the present context.

The method developed by Lan [39] is employed here to compute the downwash from Eq. (4.39). This method starts with the Weissinger velocity potential, and, placing the lifting line on the quarter-chord line, computes the downwash at the three-quarter-chord line. A brief description of this method is presented here.

Consider the first integral on the right-hand side of Eq. (4.43). This is the potential due to $\Gamma(\tilde{y})$ along the lifting line, i.e.,

$$\Phi_1 = \frac{1}{4\pi} \int_{-1}^{1} \frac{z\Gamma(\eta)}{z^2 + (y-\eta)^2} \{1 + \frac{(x-\xi)}{R}\} d\eta \qquad (4.47)$$

where $R^2 = (x-\xi)^2 + (y-\eta)^2 + z^2$ and tildes are dropped for convenience. The origin for the co-ordinate axes is assumed to be at the mid-root chord. Also,

$$\xi = - c_0/4 + m|\eta| \qquad (4.48)$$

$$x = - c_0/4 + c(y)/2 + m|y| \qquad (4.49)$$

These are introduced in Eq. (4.47), and the resulting expression is

expanded for small c(y). By retaining only first order terms in the expansion, and differentiating them with respect to z, the required expression for θ_1 (evaluated at z=0) is obtained as

$$\theta_1(x,y,0) = \frac{1}{4\pi}\int_{-1}^{1} \frac{\Gamma(\eta)}{(y-\eta)^2}\left\{1 + \frac{x-m'|\eta|}{R_1} + \frac{c(\eta)}{4}\frac{(y-\eta)^2}{R_1^3}\right\} d\eta \qquad (4.50)$$

where $m' = m-(c_0/4)(1-\lambda)$ is the tangent of the mid-chord sweep, and $R_1^2 = (x-m'|\eta|)^2 + (y-\eta)^2$. The right hand side of Eq. (4.50) is integrated by parts to arrive at the following expression for θ_1:

$$\theta_1(x,y,0) = \frac{1}{4\pi}\int_{-1}^{0} \frac{Q(\eta)}{y-\eta}\frac{d\Gamma(\eta)}{d\eta} d\eta + \frac{1}{4\pi}\int_{0}^{1} \frac{P(\eta)}{y-\eta}\frac{d\Gamma(\eta)}{d\eta} d\eta \qquad (4.51)$$

The functions $P(\eta)$ and $Q(\eta)$ are defined in [39] and details on the derivation are available in [40]. The integrals are reduced to finite sums by discretizing $\Gamma(y)$. Thus, Eq. (4.51) reduces to the following:

$$\theta_1(x_i,y_i,0) = \frac{1}{4\pi}\sum_{k=1}^{N} \Delta\Gamma(\eta_k)\left\{\frac{P(\eta_k)}{y_i-\eta_k} - \frac{Q(\eta_k)}{y_i+\eta_k}\right\} \qquad (4.52)$$

By writing $\Delta\Gamma(\eta_k) = \Gamma(y_{k+1}) - \Gamma(y_k)$, Eq. (4.52) may be expressed as

$$\theta_1(x_i,y_i,0) = \sum_{k=1}^{N} \Gamma(y_k)A(i,k) \qquad (4.53)$$

This is the required expression for the downwash due to the $\Gamma(y)$ distribution. A similar expression is obtained from the second integral on the right-hand side of Eq. (4.43), i.e.,

$$\theta_2(x_i,y_i,0) = \sum_{k=1}^{N} \Gamma_J(y_k)A(i,k) \qquad (4.54)$$

The vortex sheet behind the wing is assumed to extend downstream from the wing trailing edge. The continuous distribution $\gamma(x,y)$ is replaced with a finite number (M) of discrete vortices of strength $\gamma_\ell(y)$ located at x_ℓ, $\ell=1,2,\ldots,M$ behind the wing. Each of these vortices is further represented in the same manner as $\Gamma(y)$ is discretized, so that the jet sheet behind the wing is represented essentially by a vortex lattice. The downwash computed from this system of vortices is expressed as

$$\theta_3(x_i,y_j,0) = \sum_{\ell=1}^{M} \sum_{k=1}^{N} \gamma_\ell(y_k)B(i,j,k,\ell) \qquad (4.55)$$

Equations (4.53) - (4.55) together provide an expression for the downwash angle in terms of the unknown $\Gamma(y_k)$, $\Gamma_J(y_k)$ and $\gamma_\ell(y_k)$, $k=1,2,\ldots,N$; $\ell=1,2,\ldots,M$. This expression is used in the discretized versions of Eqs. (4.44) - (4.46), and the resulting set of simultaneous equations are solved for the unknowns.

The lift-curve slope required in Eq. (4.44) is to be obtained by solving Eq. (4.18) or the equivalent Eqs. (4.12), (4.13a) and (4.13c). However, in the present analysis, a potential flow method described in Chap. 2 has been employed for this purpose. As noted earlier, this method has been found to give results which compare reasonably well with the solution of Euler equations.

The analysis presented thus far is applicable to incompressible flows. A limited extension is made to account for the compressibility effects by introducing the Prandtl-Glauert factor $\beta = \sqrt{(1-M_\infty^2)}$ at

appropriate places in the expressions for Φ, Eq. (4.43), as well as in the lift-curve slope in Eq. (4.44). A rigorous treatment of the nonuniform compressible flow past a wing section would require the solution of the Euler equations coupled with the energy equation. However, it is observed that the nonuniformities in the slipstreams at high speeds would be relatively smaller than at low speeds. Hence, it is hoped that the Prandtl-Glauert correction, which is known to provide excellent corrections to the lift of airfoils in uniform subcritical flow, will provide a reasonable correction in the present case where the approach flow is not uniform.

4.6 Results And Discussion

The spanwise lift distribution and total lift have been computed for several configurations and compared with available experimental data. As the first example, the configuration tested by Stuper [41] is considered. In these experiments, the wing was rectangular and spanned the wind tunnel walls. The ratio of chord to geometric span was 5.25. A slipstream simulator was placed centrally ahead of the wing. The ratio of the slipstream radius to the wing chord was 0.3, and the velocity ratio of the slipstream was 1.36. Figure 4.3 shows the spanwise distribution of the incremental lift non-dimensionalized with the incremental lift as obtained by the strip theory. Present theoretical results are also shown in the figure. It is observed that there is a good agreement between the two results, particularly in the region of the slipstream. Viscous effects at the jet boundary might have contributed to the discrepancy around $(y/r)=1.0$. Experimentally measured large values of incremental lift for $(y/r)>1.0$ could not be

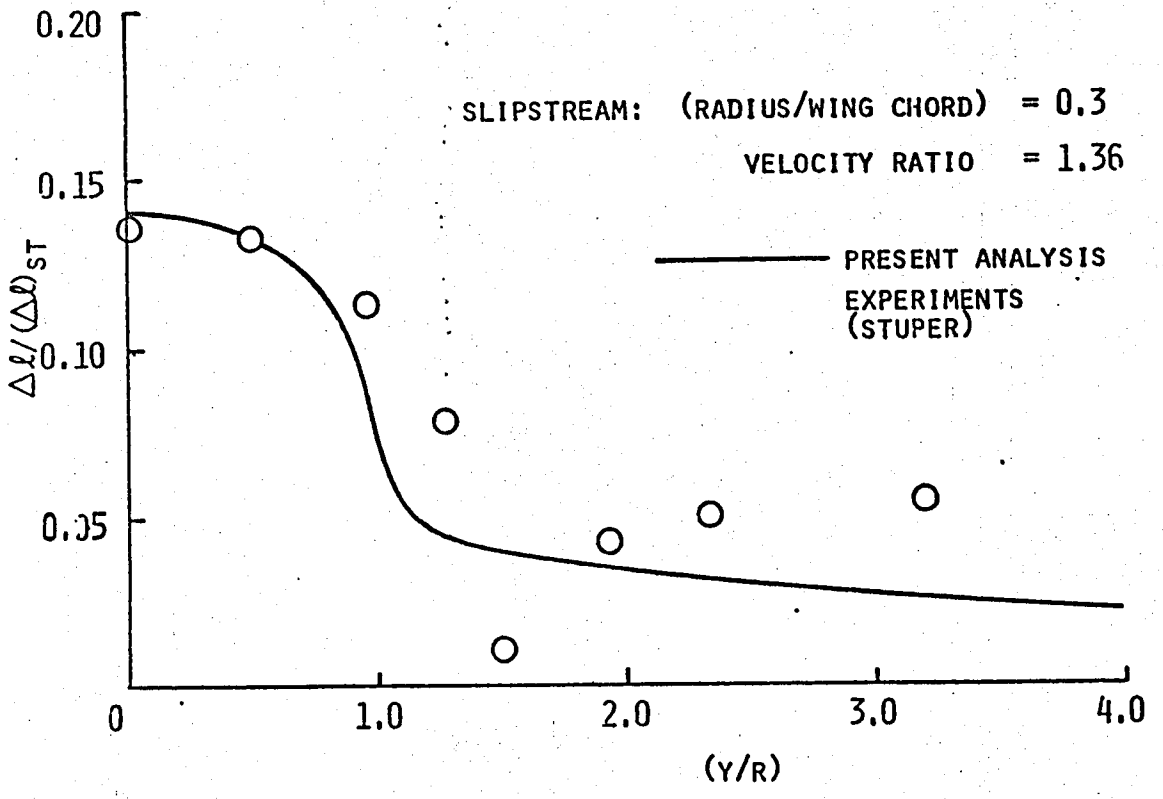

Fig. 4.3 Additional lift distribution due to slipstream on a two-dimensional wing at α = 12 degrees.

explained, but are suspected to be partly due to the tunnel wall interference.

As the second example, the configuration tested by Possio [42] is considered. In this example, the wing had an aspect ratio of 6.5 and a taper ratio of 0.5. A single model propeller was placed ahead of the wing. Several sets of data are available with varying velocity ratio and angle of attack. Figure 4.4 shows the spanwise lift distribution for the wing alone, and for the wing with the slipstreams of velocity ratio 1.4 and 1.6. In these tests only the incremental total lift coefficients were measured. The present theoretical values of ΔC_L = 0.068 and 0.098 compare very well with the corresponding experimental values of 0.07 and 0.10.

In the next example considered, the wing (tested by Maarsingh [17]) had a rectangular planform with an aspect ratio of 7.9. Two simulators were placed on each side of the wing at 42 percent and 79 percent of the semispan. The simulated slipstream radius was 0.28 times the wing chord. Test results are available for the wing alone and for the wing with slipstreams having velocity ratios of 2.0 and 3.0. Figure 4.5 shows the spanwise lift distribution for the test configurations obtained by the present analysis. The spanwise distribution of the incremental lift (Δc_ℓ) due to the jets for the two velocity ratios, compared with the experimental values in Fig. 4.6. The results computed by Maarsingh [16] using Ting's method [15] are also shown in this figure. It should be noted that the present method degenerates into Ting's method for unswept wings. However, there are some minor differences between the present results and those of Maarsingh [16]. These differences are suspected to be primarily due to the inaccurate

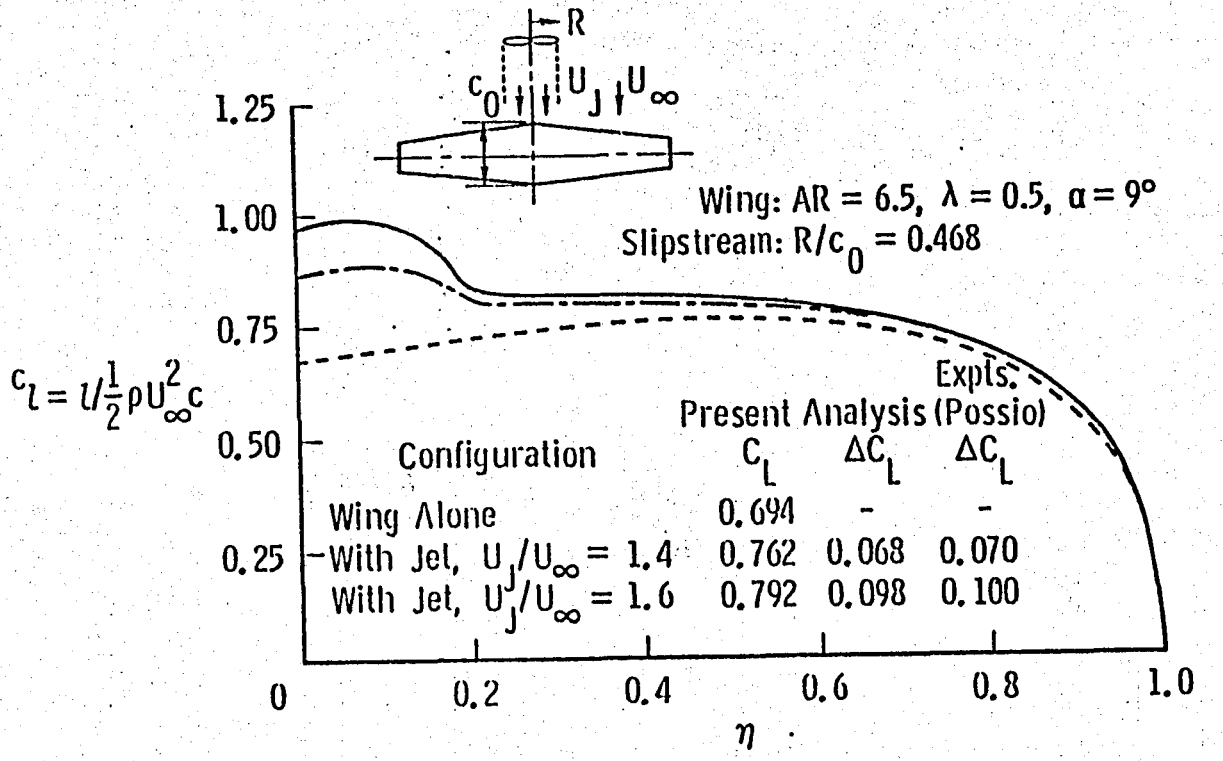

Fig. 4.4 Spanwise lift distribution with and without the slipstream on a tapered wing of AR = 6.5, λ = 0.5 at α = 9 degrees.

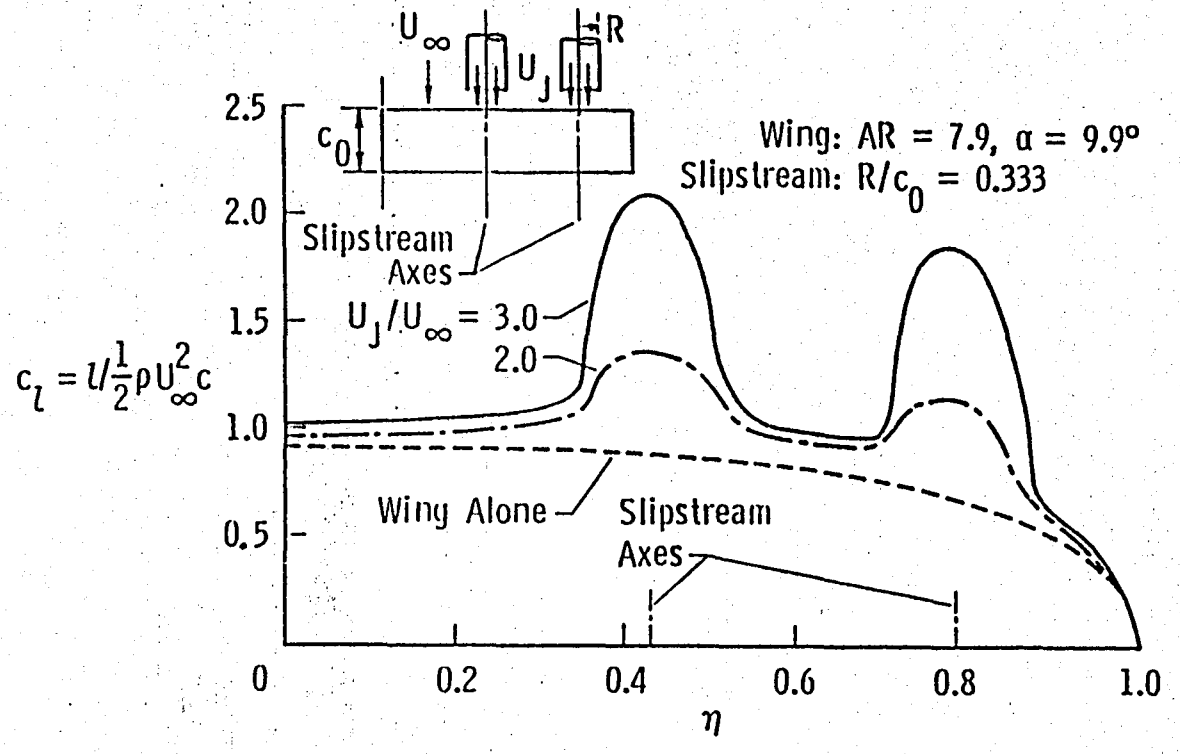

Fig. 4.5 Spanwise lift distribution with and without the slipstream on a rectangular wing of AR = 7.9 at α = 9.9 degrees.

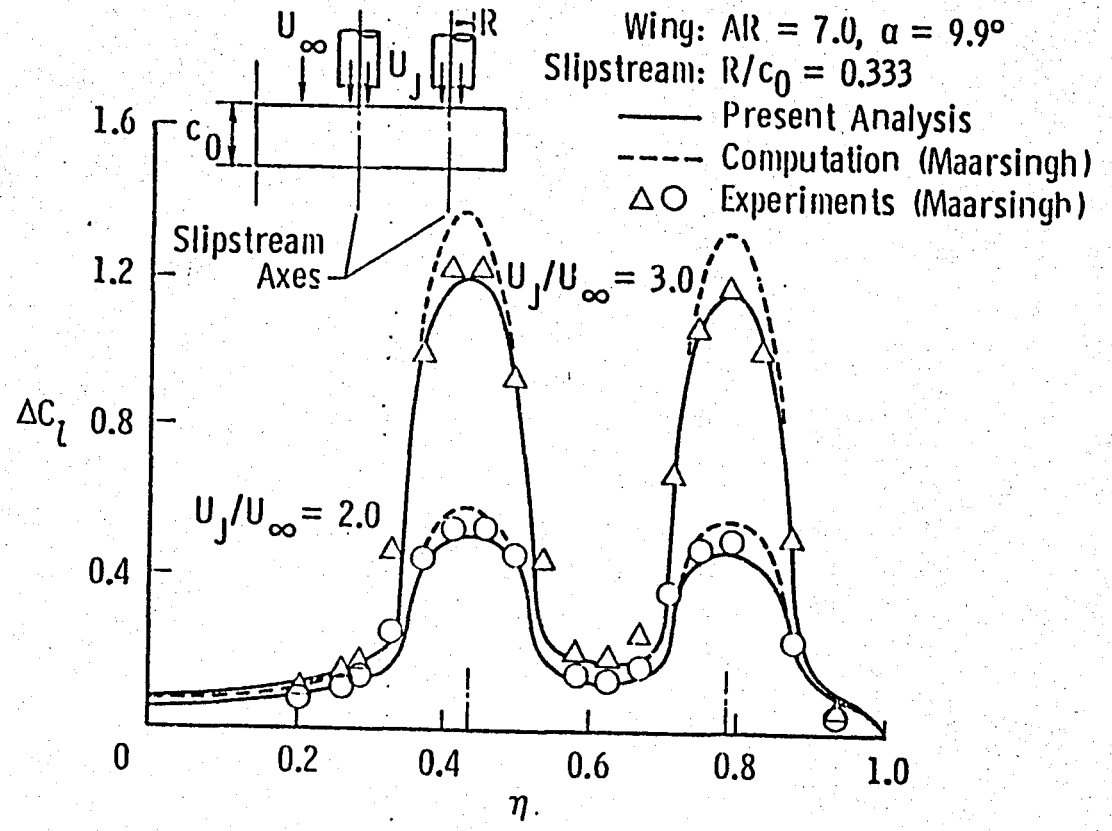

Fig. 4.6 Spanwise distribution of incremental lift due to the slipstreams on a rectangular wing of AR = 7.9 at α = 9.9 degrees.

This Page Intentionally Left Blank

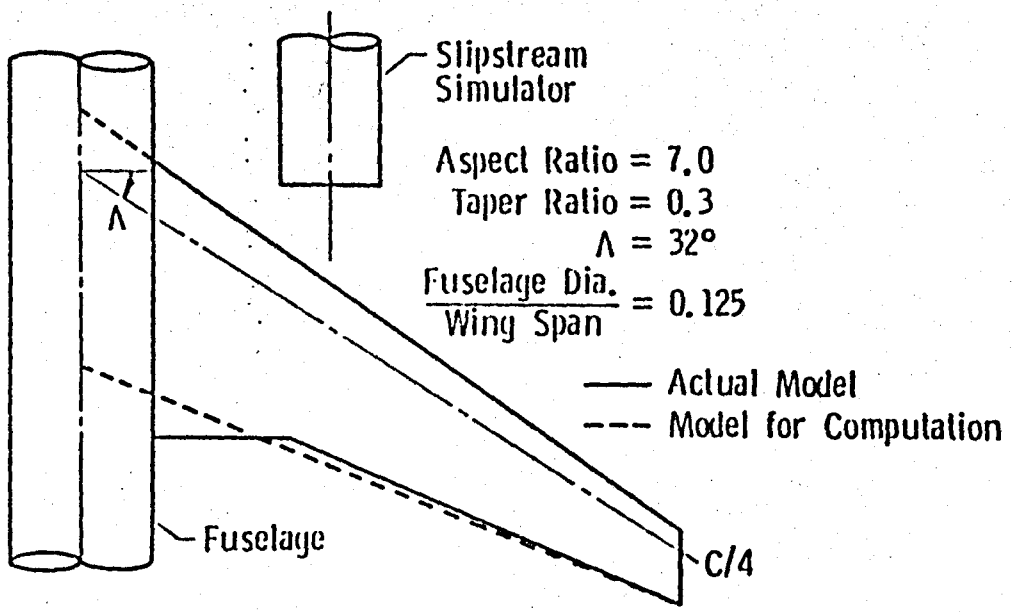

Fig. 4.7 The swept wing geometry (Helge and Crowder model).

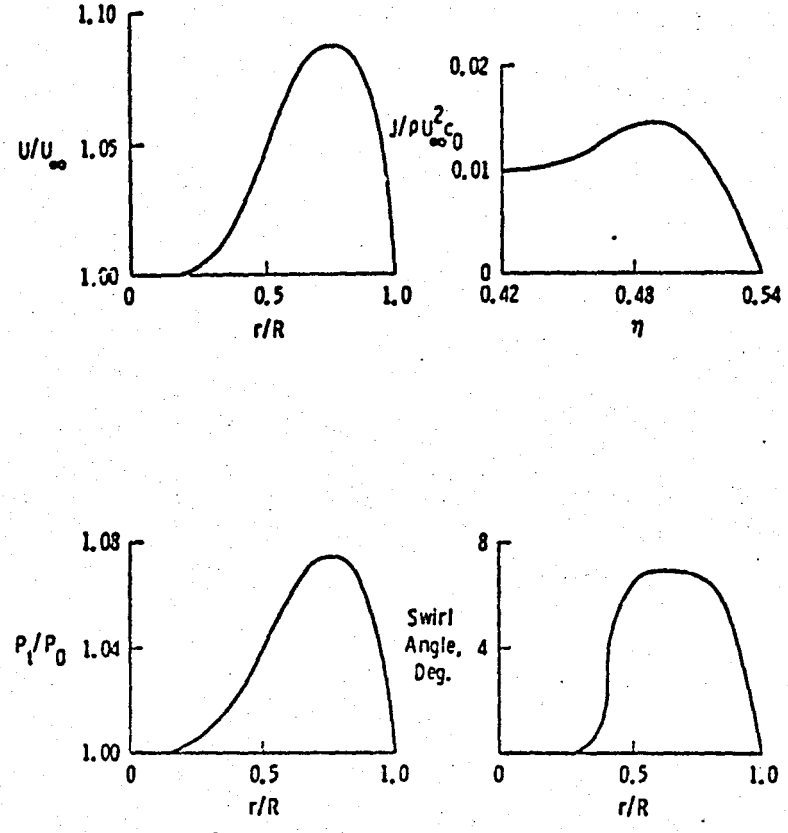

Fig. 4.8 The properties of the jet at $M_\infty = 0.8$.

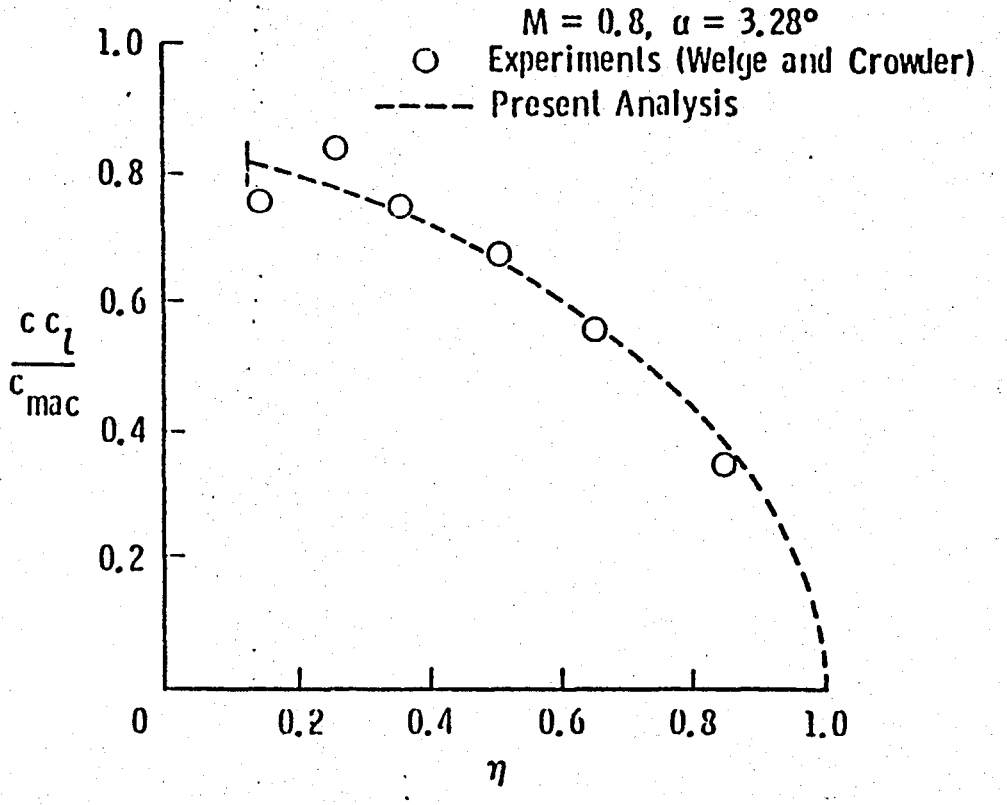

Fig. 4.9 Spanwise load distribution on the swept wing at $M_\infty = 0.8$ and $\alpha = 3.28$ degrees.

outboard stations; but the agreement is not as good at stations close to the wing root. It should be noted that the test configuration had a body at the center, and the wing planform was modified near the wing root. These details were not simulated in the present analysis. Some of the differences between the present results and the experimental data at the inboard stations may be attributed to these modeling difficiencies.

The effect of the jet without swirl on the spanwise load distribution at M_∞ = 0.8 and α = 3 degrees is illustrated in Fig. 4.10. The experimental data, the results obtained by the present analysis, and the solution of Euler equations [26] are included in this figure. It should be noted that the jet is a rather weak jet with a maximum total pressure ratio of 1.075. As a result, it does not modify the load distribution significantly. It can be observed from the figure that the incremental lift values obtained by the present analysis agree closely with the experimental data. A comparison of the Euler solution [27] with experimental data shows a trend similar to that which was observed earlier - at the wing inboard stations there is good agreement, but at the outboard stations there is some discrepancy. Nevertheless, the incremental lift values obtained by this method also compare well with the experimental data.

The effect of the swirl in the jet on the spanwise load distribution at M_∞ = 0.8 and α = 3 degrees is illustrated in Fig. 4.11. The experimental data are available for the wing with jet having nominal swirl angles of 7 degrees up inboard, and 7 degrees down inboard. These experimental data are shown in Fig. 4.11a and 4.11b for the up inboard and down inboard swirl distributions respectively. Present results and

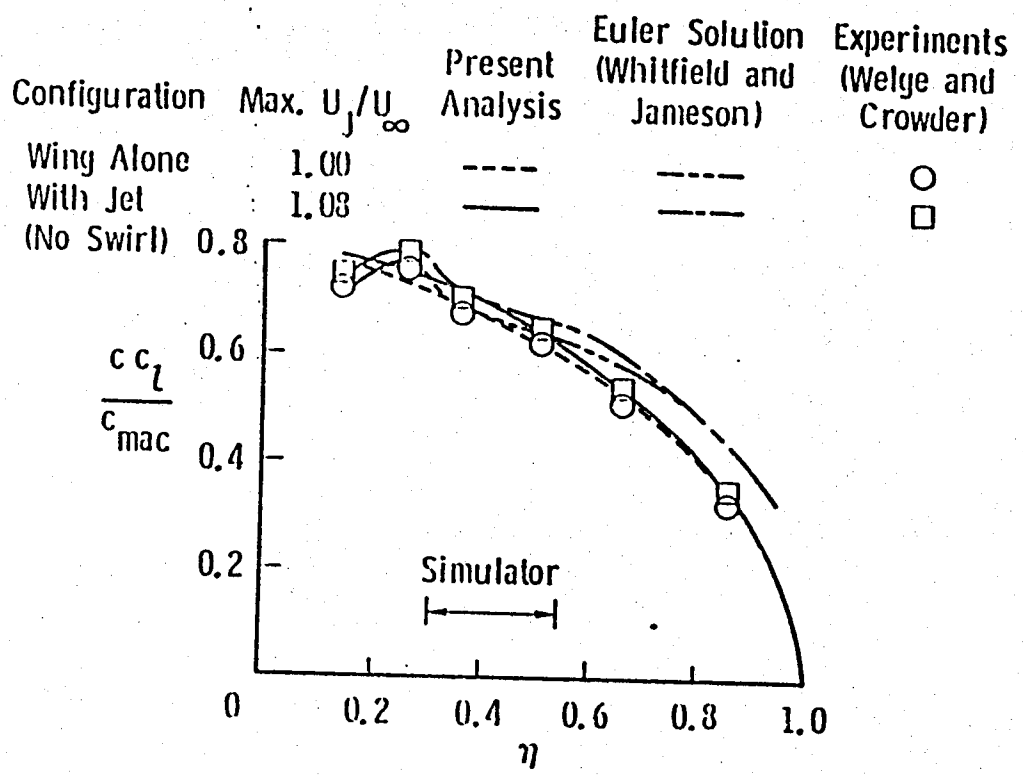

Fig. 4.10 Spanwise load distribution on the swept wing with and without the simulator at $M_\infty = 0.8$ and $\alpha = 3$ degrees.

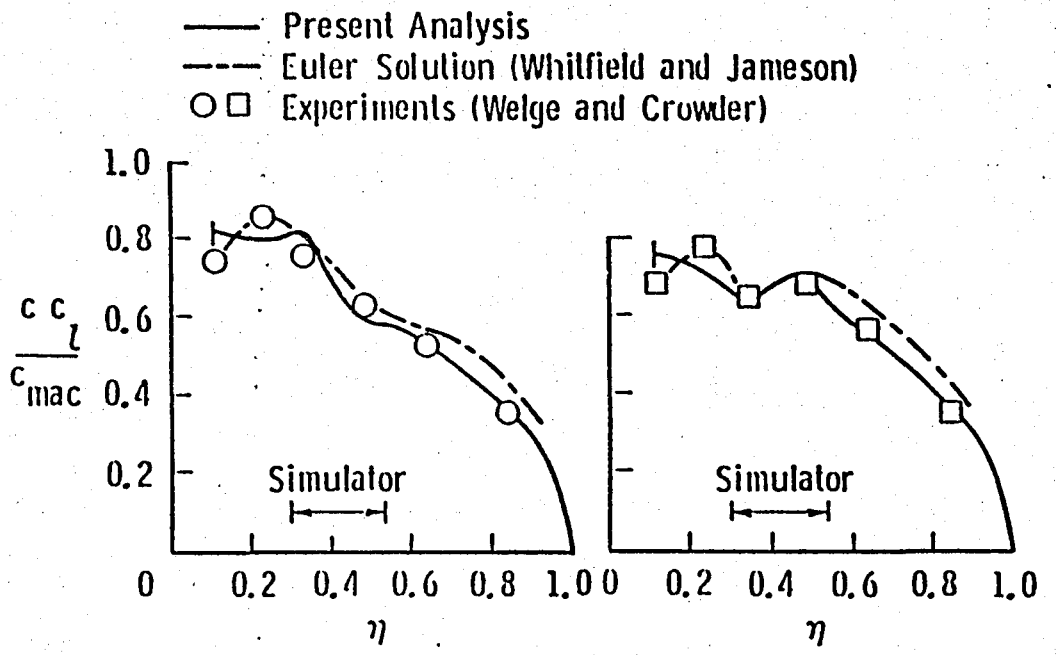

Fig. 4.11 Effect of the swirl on the spanwise load distribution on the swept wing at $M_\infty = 0.8$ and $\alpha = 3$ degrees.

the computed results from [26] are also included in these figures which bring out the interesting effect of the swirl in the slipstream on the spanwise load distribution. Quantitative agreement between the Euler solution [26] and the experiments is good at stations close to the wing root; the agreement is not as good at the outboard stations. In contrast, a comparison of the present results with the experiments shows a good agreement at the outboard stations but the agreement is not as good at stations close to the wing root. This discrepancy in the results near the wing root may be attributed to the differences between the theoretical model used in the present analysis and the actual wind tunnel model. A closer examination of figures reveals that the present results agree with experimental data qualitatively; but quantitatively, the present analysis seems to slightly overpredict the effect of the swirl.

Chapter 5

CONCLUDING REMARKS

The small perturbation potential flow theory has been applied to the problem of determining the chordwise pressure distribution and lift of thin airfoils in nonuniform parallel streams with stepped velocity profiles. The method has been extended to the case of an undisturbed stream having a given smooth velocity profile with no velocity discontinuities. The analysis is based on the method of images, and allows for potential disturbances in a rotational undisturbed flow. Several examples are considered and the present potential solutions obtained by different approximations are compared with the Euler solutions. The results indicate that although approximate, the present method yields results which bring out the effect of the interference problem, while avoiding the need to solve the Euler equation. In the present analysis the thickness effects have been neglected for the purpose of computing the airfoil pressure distribution. The effect of airfoil thickness can in principle be included, but would require further analysis.

The classical lifting-line theory for the interference of wing and propeller slipstream has been modified in Chap. 3. The classical theory assumes that the slipstream is in the form of a circular cylinderical jet with a velocity jump across this cylinder. In the present analysis, this assumption has been dropped, and the velocity distribution is

assumed to have a given smooth profile with no velocity discontinuities. The lift distribution in the examples considered here demonstrated that whereas the total lift may not be affected by the assumption of a uniform velocity profile for the slipstream, the distributions could be very different in the two cases. The present modification to the classical theory brings out the effects of the nonuniformity on the spanwise lift and indeed drag distributions.

The method of analysis developed here can also be extended to the case of a wing in multiple nonoverlapping slipstreams. However, it is well known that the lifting line theory overpredicts the lift due to the slipstream. This is due to the fact that, while accounting for the effects of the slipstream boundary, the trailing vortices are assumed to extend to infinity in both directions. This discrepancy was recognized and corrected in the development of lifting surface theories. The lifting surface theories produce good results, but are applicable only to slipstream in which the velocity is uniform. The present method can be extended to the lifting surface theories as well as to the lattice methods applied to the wing-slipstream interference problem.

The problem of the interference of multiple propeller slipstreams with large aspect ratio swept wings has been treated in Chap. 4 by the method of asymptotic expansions. Although this is only a first order theory, the important second order contributions from the propeller slipstream have been included in the analysis. The method is quite versatile in the sense that it can handle slipstreams of any given velocity distribution. The time dependence of the velocity field in the slipstream is neglected. The increased axial velocity and the swirl component in the slipstream are of primary concern in the present

analysis. One of the assumptions that the spanwise extent of the slipstream was of the order of the wing span, was not satisfied in the examples considered; but the results do not seem to be affected noticeably. Viscous effects are neglected; but the compressibility effect is accounted for by the Prandtl-Glauert factor.

Several examples are considered for which experimenal data are available, and in each case the spanwise lift distribution is obtained by the present method, and compared with the corresponding experimental data. In most of the cases the agreement between the two results is very good. In the first example, the differences between the experimental data and the present results are suspected to be partly due to the tunnel wall interference in the measurements. In the last example considered, the experimental configuration had a body on the centerline; also the wing planform was modified near the wing root. These details were not simulated in the present analysis. It is suspected that these differences have resulted in the difference in the two sets of results.

In the present analysis, the effect of the swirl in the slipstream is accounted for by assuming that the swirl only changes the local angle of attack. This approach yields results which compare well qualitatively with the experimental data. However, the method seems to slightly overpredict the effect of swirl on the spanwise load distribution.

A comparison was made between the present results and the numerical solution of Euler equations. The numerical solution of Euler equations requires a large computer memory and extensive computing effort. For

example, the computer program developed by Whitfield and Jameson [24] required 900,000 words of memory, and 341 seconds computing time on Cray-15 computer for a relatively coarse (96x16x16) grid. This grid provided results for only 6 stations along the wing semispan. This method, however, provides details of the flowfield in the entire computational domain. In contrast, the present method is simple, and requires relatively small computational effort. For example, the computer code developed to compute the spanwise load distribution using the present method required 130,000 words of memory, and about 40 seconds of computing time on CDC Cyber 175 computer, and provided the results at 40 stations along the wing semispan. The spanwise lift distribution obtained by the present method compared favorably with experimental data.

REFERENCES

1. Ludemann, S. G., "Prop-fan Powered Aircraft - An Overview," Society of Automotive Engineers, Paper No. 820957, Paper presented at the West Coast International Meeting, San Francisco, California, August 1982.

2. Williams, L. J., "Small Transport Aircraft Technology," NASA SP-460, 1983.

3. Arndt, W. E., "Fuel Efficient And Mach 0.8 Too," Lockheed Horizon, Issue 10, Spring 1982, pp. 26-34.

4. Smelt, R. and Davies, H., "Estimation of Increase in Lift Due to Slipstream," British Aeronautical Research Council, Reports and Memoranda 1788, 1937.

5. Millikan, C. B., "The Influence of Running propellers on Airplane Characteristics," Journal of Aeronautical Sciences, Vol. 7, No. 3, January 1940, pp.85-106.

6. Koning, C., "Influence of the Propeller on other Parts of the Airplane Structure," Aerodynamic Theory, Vol. IV, Edited by W. F. Durand, Division M, Dover Publication, New York, 1963.

7. Ferrari, C., "Propellers and Wing Interaction at Subsonic Speeds," Aerodynamics Component of Aircraft at High Speed, Edited by A. F. Donovan and H. C. Lawrence, Sec. D, Ch. 3. Princeton University Press, Princeton, New Jersey, 1957.

8. Ting, L. and Liu, C. H., "Thin Airfoil in Nonuniform Parallel Streams," New York University Report AA 68-20, New York University, July 1968, Also Journal of Aircraft, Vol. 6, No. 2, March-April 1969, pp. 173-175.

9. Chow, F., Krause, E., Liu, C. H. and Mao, J., "Numerical Investigations of an Airfoil in a Nonuniform Stream," Journal of Aircraft, Vol. 7, No. 6, November-December 1970, pp. 531-537.

10. Kleinstein, G. and Liu, C. H., "Application of Airfoil Theory for Nonuniform Streams to Wing-Propeller Interaction," Journal of Aircraft, Vol. 9, No. 2, February 1972, pp. 137-142.

11. Rethorst, S., "Lift on a Wing in a Propeller Slipstream as Related to Low-Speed Flight," Aeronautical Engineering Review, October 1958, pp. 42-48.

12. Wu, T. Y. and Talmadge, R. B., "A Lifting Surface Theory for Wings Extending Through Multiple Jets," Report No. 8, Vehicle Reserch Corporation, Pasadena, California, August 1961.

13. Cumberbatch, E., "A Lifting Surface Theory for Wings at Angles of Attack Extending Through Multiple Jets," Report No. 9, Vehicle Research Corporation, Pasadena, California, July 1963.

14. Jameson, A., "Analysis of Wing Slipstream Interaction," NASA CR-1632, August 1970.

15. Ting, L., Liu, C. H., and Kleinstein, G., "Interference of Wing and Multiple Propellers," AIAA Paper 71-614, Presented at the AIAA 4th Fluid and Plasma Dynamics Conference, Palo Alto, California, 1971; Also AIAA Journal, Vol. 10, No. 7, July 1972, pp. 906-914.

16. Maarsingh, R. A., "Calculation of the Lift Distribution on a Wing in Jets or Slipatreams using Ting's Method," NLR TR 73151C, National Aerospace Laboratory, Netherlands, October 1973.

17. Maarsingh, R. A., "Evaluation of Ting's Method for the Calculation of the Lift Distribution on a Wing in Propulsive Jets," NLR TR 80078U, National Aerospace Laboratory, Netherlands, November 1979.

18. Rioner, H. S. and Ellis, N. D., "Aerodynamics of Wing Slipstream Interaction," Transactions of the Canadian Aeronautics and Space Institute, Vol. 5, No. 2, September 1972, pp. 56-63.

19. Lan, C. E., "Wing-Slipstream Interaction with Mach Number Nonuniformity," Journal of Aircraft, Vol. 12, No. 10, October 1975, pp. 759-760.

20. Levinsky, E. S., Thommen, H. U., Yager, P. M., and Holland, C. H., "Lifting-Surface Theory for V/STOL Aircraft in Transition and Cruise, Part I," Journal of Aircraft, Vol. 6, No. 6, November - December 1969, pp. 488-495.

21. Levinsky, E. S., Thommen, H. U., Yager, P. M., and Holland, C. H., "Lifting-Surface Theory for V/STOL Aircraft in Transition and Cruise, Part II," Journal of Aircraft, Vol. 7, No. 1, January - February 1970, pp. 58-65.

22. Rizk, M. H., "Propeller Slipstream/Wing Interaction in the Transonic Regime," AIAA Paper 80-0125, Presented at the AIAA 18th Aerospace Science Meeting, Pasadena, California, January 1980.

23. Chandrasekaran, B. and Bartlett, G., "Method for Calculating Effects of a Propfan on Aircraft Aerodynamics at Subsonic Speeds," AIAA Paper 83-1216, Presented at the AIAA/SAE/ASME 19th Joint Propulsion Conference, Seattle, Washington, June 1983.

24. Narain, J. P., "A Transonic Analysis of Propfan Slipstream Effects on a Supercritical Wing," AIAA Paper 83-0186, Presented at the AIAA 21st Aerospace Sciences Meeting, Reno, Nevada, January 1983.

25. Samant, S. S., Yu, N.J., and Rubbert, P. E., "Transonic Flow Simulation of Prop-Fan Configurations," AIAA Paper 83-0187, Presented at the AIAA 21st Aerospace Sciences Meeting, Reno, Nevada, January 1983.

26. Welge, H. R. and Crowder, J. P., "Simulated Propeller Slipstream Effects on a Supercritical Wing," NASA CR-152138, June 1978.

27. Whitfield, D. L. and Jameson, A., "Three-dimensional Euler Equation Simulation of a Propeller-Wing Interaction in Transonic Flow," AIAA Paper 83-0236, Presented at the AIAA 21st Aerospace Sciences Meeting, Reno, Nevada, January 1983.

28. Van Dyke, M., "Lifting Line Theory as a Singular Perturbation Problem," SUDAER No. 165, Stanford University, Stanford, California, August 1963.

29. Anderson, W. K., Thomas, J. L., and Van Leer, B., "Finite Volume Flux Vector Splitting for the Euler Equations," AIAA Paper 85-0122, to be presented at the AIAA 23rd Aerospace Sciences Meeting, Reno, Nevada, January 1985.

30. Von Karman, T., "Beitrag zur Theorie des Auftriebes," Vortrage aus dem Gebiete der Aerodynamik und Verwandter Gebiete, Aachen, 1929.

31. Glauert, H., "The Influence of a Uniform Jet on the Lift of an Airfoil," British Aeronautical Research Committee, Reports and Memoranda 1602, 1934.

32. Lan, C. E., "Quasi-Vortex-Lattice Method in Thin Wing Theory," Journal of Aircraft, Vol. 6, No. 2, 1969, pp. 173-175.

33. Kerney, K. P., "A Theory of High Aspect Ratio Jet Flap," AIAA Journal, Vol. 9, No. 3, March 1971, pp. 431-435.

34. Tokuda, N., "An Aysmptotic Theory of the Jet Flap in Three Dimensions," Journal of Fluid Mechanics, Vol. 46, Part 4, 1971, pp. 705-726.

35. Van Dyke, M., Perturbation Methods in Fluid Mechanics, The Parabolic Press, Stanford, California, 1975.

36. Cheng, H. K., Meng, S. Y., Chow, R., and Smith, R.C., "Transonic Swept Wing Studied by the Lifting Line," AIAA Journal, Vol. 19, No. 8, August 1981, pp. 961-968.

37. Cheng, H. K., Chow, R., and Melnik, R. E., "Lifting Line Theory of Swept Wing Based on Full Potential Theory," Journal of Applied Mathematics and Physics, Vol. 31, 1981, pp. 481-496.

38. Thurber, J., "An Asymptotic Method for Determining the Lift Distribution on a Swept-back Wing of Finite Span," Communications on Pure and Applied Mathematics, Vol. 18, 1965, pp. 733-756.

39. Lan, C. E. and Fasce, M. H., "Application of an Improved Nonlinear Lifting Line Theory," Journal of Aircraft, Vol. 14, No. 4, April 1977, pp. 404-407.

40. Fasce, M. H., "Application of a Improved Nonlinear Lifing Line Theory," M.S. Thesis, Department of Aerospace Engineering, University of Kansas, March 1975.

41. Stuper, J., "Effects of Propeller Slipstream on Wing and Tail," NACA TM No. 874, 1938.

42. Possio, C., "Experimental Investigation of Propeller Wing Interference," Aerotecnica, Vol. 26, 1946, pp. 73-77.

END

DATE

FILMED

JUL 9 1985

End of Document